

**Photoelectron spectroscopy and theoretical studies of gaseous uranium hexachlorides in different oxidation states:  $UCl_6^{q-}$  ( $q = 0-2$ )**

Jing Su, Phuong D. Dau, Hong-Tao Liu, Dao-Ling Huang, Fan Wei, W. H. E. Schwarz, Jun Li, and Lai-Sheng Wang

Citation: *The Journal of Chemical Physics* **142**, 134308 (2015); doi: 10.1063/1.4916399

View online: <http://dx.doi.org/10.1063/1.4916399>

View Table of Contents: <http://scitation.aip.org/content/aip/journal/jcp/142/13?ver=pdfcov>

Published by the [AIP Publishing](#)

---

**Articles you may be interested in**

[Strong electron correlation in  \$UO\_2\$  –: A photoelectron spectroscopy and relativistic quantum chemistry study](#)  
*J. Chem. Phys.* **140**, 094306 (2014); 10.1063/1.4867278

[Photoelectron spectroscopy and theoretical studies of  \$UF\_5\$  – and  \$UF\_6\$  –](#)  
*J. Chem. Phys.* **136**, 194304 (2012); 10.1063/1.4716182

[Theoretical study of structure and photoelectron spectroscopy of  \$In\_xP\_y\$  – and  \$In\_xP\_y\(x+y=6\)\$  clusters](#)  
*J. Chem. Phys.* **124**, 184316 (2006); 10.1063/1.2194553

[On the structure and chemical bonding of  \$Si\_6^{2-}\$  and  \$Si\_6^{2-}\$  in  \$NaSi\_6\$  – upon  \$Na^+\$  coordination](#)  
*J. Chem. Phys.* **124**, 124305 (2006); 10.1063/1.2177254

[A study of the structure and bonding of small aluminum oxide clusters by photoelectron spectroscopy:  \$Al\_xO\_y\$  – \( \$x=1-2\$ ,  \$y=1-5\$ \)](#)  
*J. Chem. Phys.* **106**, 1309 (1997); 10.1063/1.474085

---

How can you **REACH 100%**  
of researchers at the Top 100  
Physical Sciences Universities? (TIMES HIGHER EDUCATION RANKINGS, 2014)

With *The Journal of Chemical Physics*.

**AIP** | The Journal of  
Chemical Physics

THERE'S POWER IN NUMBERS. Reach the world with AIP Publishing.



# Photoelectron spectroscopy and theoretical studies of gaseous uranium hexachlorides in different oxidation states: $\text{UCl}_6^{q-}$ ( $q = 0-2$ )

Jing Su,<sup>1,2,a)</sup> Phuong D. Dau,<sup>3,a)</sup> Hong-Tao Liu,<sup>1,3</sup> Dao-Ling Huang,<sup>3</sup> Fan Wei,<sup>2</sup>  
 W. H. E. Schwarz,<sup>2,b)</sup> Jun Li,<sup>2,c)</sup> and Lai-Sheng Wang<sup>3,c)</sup>

<sup>1</sup>Shanghai Institute of Applied Physics, Chinese Academy of Sciences, Shanghai 201800, China

<sup>2</sup>Department of Chemistry and Key Laboratory of Organic Optoelectronics and Molecular Engineering of the Ministry of Education, Tsinghua University, Beijing 100084, China

<sup>3</sup>Department of Chemistry, Brown University, Providence, Rhode Island 02912, USA

(Received 10 January 2015; accepted 17 March 2015; published online 6 April 2015)

Uranium chlorides are important in actinide chemistry and nuclear industries, but their chemical bonding and many physical and chemical properties are not well understood yet. Here, we report the first experimental observation of two gaseous uranium hexachloride anions,  $\text{UCl}_6^-$  and  $\text{UCl}_6^{2-}$ , which are probed by photoelectron spectroscopy in conjunction with quantum chemistry calculations. The electron affinity of  $\text{UCl}_6$  is measured for the first time as +5.3 eV; its second electron affinity is measured to be +0.60 eV from the photoelectron spectra of  $\text{UCl}_6^{2-}$ . We observe that the detachment cross sections of the 5f electrons are extremely weak in the visible and UV energy ranges. It is found that the one-electron one-determinantal molecular orbital picture and Koopmans' theorem break down for the strongly internally correlated U-5f<sup>2</sup> valence shell of tetravalent  $\text{U}^{+4}$  in  $\text{UCl}_6^{2-}$ . The calculated adiabatic and vertical electron detachment energies from *ab initio* calculations agree well with the experimental observations. Electronic structure and chemical bonding in the uranium hexachloride species  $\text{UCl}_6^{2-}$  to  $\text{UCl}_6$  are discussed as a function of the oxidation state of U. © 2015 AIP Publishing LLC. [<http://dx.doi.org/10.1063/1.4916399>]

## I. INTRODUCTION

Uranium halides play essential roles both in fundamental actinide chemistry and in nuclear technologies from uranium enrichment to separation. Among the most studied actinide complexes are the uranium hexahalides, possessing octahedral symmetry and thereby providing a well-defined platform for theoretical investigations.<sup>1-3</sup> The  $[\text{UCl}_6]^{2-}$  dianion is the most important species when tetravalent uranium compound ( $\text{U}^{+4}$ )Cl<sub>4</sub> is dissolved in LiCl/KCl molten salt. It has been shown that trivalent  $\text{U}^{+3}$  and pentavalent  $\text{U}^{+5}$  are formed during redox processes.<sup>4-6</sup> The  $[\text{UCl}_6]^{3-}$  and  $[\text{UCl}_6]^-$  species have also been observed in room-temperature ionic liquids.<sup>7</sup> Even though there have been many experimental and computational studies of  $[\text{U}(\text{f}^1)\text{Cl}_6]^-$  in condensed phases,<sup>1,8-16</sup> the accurate account of the electronic structure of the  $[\text{U}(\text{f}^2)\text{Cl}_6]^{2-}$  species has been challenging owing to the highly complex f<sup>2</sup> system and the perturbations caused by interactions with the counterions in crystal and solution phases.<sup>17-21</sup>

Anion photoelectron spectroscopy (PES) is a powerful experimental technique to probe the ground and excited states of neutral species, through electron detachment from singly charged anions. We have developed PES techniques to study solution-phase species, both singly charged and multiply charged anions, in the gas phase using electrospray ionization

(ESI).<sup>22</sup> In particular, our recent development of a cryogenic ion trap has allowed the creation of vibrationally cold anions,<sup>23</sup> making it possible for high-resolution spectroscopic investigations of solution anions in the gas phase.<sup>24</sup> Relevant to the current uranium halides, we have successfully applied ESI-PES to probe the electronic structures of a series of uranyl and uranium halide anions in conjunction with relativistic quantum chemical calculations.<sup>25-31</sup> In particular, we have produced  $[\text{UF}_5]^-$  and  $[\text{UF}_6]^-$  using ESI and obtained the PES spectra of  $[\text{UF}_5]^-$  both at room temperature and low temperature, which yielded an accurate electron affinity (EA) for  $\text{UF}_5$  as  $3.885 \pm 0.015$  eV.<sup>28,29</sup> The  $[\text{U}(\text{f}^2)\text{F}_5]^-$  anion has a C<sub>4v</sub> symmetry with two unpaired 5f electrons, occupying f<sub>z<sup>2</sup></sub> and f<sub>xyz</sub> type orbitals, respectively. We found that the detachment cross section of the f<sub>xyz</sub> electron is at least a factor of ten smaller relative to that of the f<sub>z<sup>2</sup></sub> electron. Consequently, we were not able to obtain the PES spectrum of  $[\text{UF}_6]^-$ , because the extra electron occupies the f<sub>xyz</sub>-type orbital of  $\text{UF}_6$  and its detachment cross section is too weak to be observed at the available photon energies.<sup>28</sup> We have also recently reported a PES and computational study of  $[\text{UCl}_5]^-$  that was produced using ESI.<sup>31</sup> In addition to weak detachment features from the 5f electrons, we were able to observe strong detachment features from the Cl 3p orbitals, whereas the electron binding energies of the F 2p electrons are too high to be observed at the available detachment photon energies in the case of  $[\text{UF}_5]^-$ . The EA of  $\text{UCl}_5$  was measured to be  $4.76 \pm 0.03$  eV, significantly higher than that of  $\text{UF}_5$ .

In the current article, we report the first experimental observation and characterization of gaseous  $[\text{UCl}_6]^-$  and

<sup>a)</sup>J. Su and P. D. Dau contributed equally to this work.

<sup>b)</sup>Mailing address: Physical and Theoretical Chemistry, University of Siegen, Siegen 57068, Germany.

<sup>c)</sup>Electronic addresses: junli@tsinghua.edu.cn and lai-sheng\_wang@brown.edu

$[\text{UCl}_6]^{2-}$  by ESI-PES, allowing us to measure successfully both the first and second EA of  $\text{UCl}_6$ . In addition, we have investigated the electron detachment energies of  $[\text{UCl}_6]^{q-}$  ( $q = 1, 2$ ) theoretically using relativistically corrected density functional theory (DFT) and *ab initio* wavefunction theories (WFT) and compared the computational data with the experimental results. The observation of the  $[\text{UCl}_6]^{2-}$  dianion is particularly interesting, as it provides long-sought gas-phase information regarding the  $f^2$  uranium(IV) hexahalides. The electronic structure and chemical bonding in the hexachlorides are investigated as a function of the uranium oxidation states from  $[(\text{U}^{+4})\text{Cl}_6]^{2-} \rightarrow [(\text{U}^{+5})\text{Cl}_6]^{-} \rightarrow [(\text{U}^{+6})\text{Cl}_6]^0$ . The current results provide further insights into the chemical and physical properties of uranium chloride anionic species, which are common in high-temperature molten salts and electrolytes.<sup>32</sup>

## II. EXPERIMENTAL AND COMPUTATIONAL METHODOLOGY

### A. Electrospray photoelectron spectroscopy with a temperature-controlled ion trap

The PES-ESI apparatus used for this study was described in detail previously.<sup>22</sup> It consisted of an ESI source and a magnetic-bottle photoelectron analyzer (the magnetic field in the interaction zone was estimated to be  $\sim 800$  gauss). It was modified by shortening the electron flight tube from 4.0 m to 2.5 m, only resulting in a slight decrease of the electron energy resolution.<sup>33</sup> The  $[\text{UCl}_6]^{-}$  and  $[\text{UCl}_6]^{2-}$  anions were produced by ESI, using a 1 mM solution of  $\text{UCl}_4$  in acetonitrile. A radio frequency quadrupole device guided the anions from the ESI source into a cryogenically controlled ion trap,<sup>23,29</sup> where the anions were accumulated and cooled for 0.1 s before being pulsed into the extraction zone of a time-of-flight mass spectrometer. The ion trap can be cooled down to 4.4 K using a closed-cycle helium refrigerator<sup>29</sup> and was operated at 20 K for the current experiment. Under our ESI conditions, both the  $[\text{UCl}_6]^{-}$  and  $[\text{UCl}_6]^{2-}$  anions were readily observed. They were selected by a mass gate and decelerated before being intercepted by a laser beam in the detachment region of a magnetic-bottle photoelectron analyzer. Four different laser wavelengths were used: 157 nm (7.866 eV) from an  $\text{F}_2$  excimer laser, 213 nm (5.821 eV) from a dye laser, 266 nm (4.661 eV), and 355 nm (3.496 eV) from a Nd:YAG laser. The PES spectra were calibrated using the known spectra of  $\text{Au}^{-}$  (2.3086 eV) and  $\text{I}^{-}$  (3.0590 eV).<sup>34,35</sup> The  $\text{Au}^{-}$  anion was produced by ESI of a pyridine solution of  $\text{PPh}_3\text{AuCl}$  and  $\text{NaSCH}_3$  with a trace amount of  $\text{CH}_3\text{OH}$ .<sup>36</sup> The electron kinetic energy resolution of the current magnetic-bottle electron analyzer was about 3%, i.e., 30 meV for 1 eV electrons.<sup>33</sup>

### B. Computational details

The theoretical studies were performed using both DFT and WFT methods. The computational details of the two kinds of methods are described separately below.

In the case of DFT calculations, we used the generalized gradient approximation (GGA) with the Perdew-Burke-Ernzerhof (PBE) functional,<sup>37</sup> as implemented in

ADF 2010.02.<sup>38–40</sup> Slater basis sets of triple- $\zeta$  plus two polarization functions (TZ2P)<sup>41</sup> were applied. The frozen core approximation for the inner shells [ $1s^2-5d^{10}$ ] of U (corresponding to 14 electrons in the 5f-6s-6p-7s (semi-) valence shell) and [ $1s^2-2p^6$ ] of Cl (with 7 electrons in the 3s3p valence shell) was applied by taking the core orbitals from free atom calculations. The scalar relativistic (SR) and spin-orbit (SO) coupling effects were taken into account by the zero order regular approximation (ZORA).<sup>42</sup> The geometries were optimized at the SR-ZORA level, and single-point energy calculations were performed with inclusion of the SO coupling effects via the SO-ZORA approach. The vibrational frequencies of  $[\text{UCl}_6]^{q-}$  ( $q = 0-2$ ) at their optimized octahedral structures were calculated at the SR DFT/PBE level. Preliminary SO-ZORA calculations show that the Jahn-Teller (JT) distortion of the open-shell species is quenched by SO interaction. For the vertical detachment energies (VDEs) of  $[\text{UCl}_6]^{-}$ , the time-dependent DFT (TDDFT) approach was used to calculate the excited states of  $\text{UCl}_6$  at the DFT/PBE ground state geometry of  $[\text{UCl}_6]^{-}$ . In the TDDFT calculations, both the B3LYP potential<sup>43,44</sup> and the “statistically averaged orbital potential” (SAOP) with the correct asymptotic  $1/r$  behavior were used.<sup>45</sup>

In the case of WFT calculations, we used the advanced *ab initio* electron correlation methods in the MOLPRO 2012.1 and NWChem 6.0 program packages.<sup>46,47</sup> With MOLPRO, we used the coupled-cluster approach with single and double and perturbative triple substitutions [CCSD(T)]<sup>48</sup> and the complete-active-space multi-configuration approach with second-order perturbation theoretical correction (CASPT2).<sup>49</sup> With NWChem, we employed the completely renormalized equation-of-motion CCSD(T) [CR-EOM-CCSD(T)] approach to calculate the excited states.<sup>50</sup> For U, the Stuttgart energy-consistent relativistic small-core pseudopotential ECP60MWB (32 electrons in the 5s5p5d6s6p5f6d7s extended valence shell) was applied with the ECP60MWB\_SEG basis.<sup>51–53</sup> For Cl, the all-electron augmented polarized valence-double- $\zeta$  basis set (aug-cc-pVDZ) was used.<sup>54</sup> The geometric structures of  $\text{UCl}_6^{2-}$  and  $\text{UCl}_6^{-}$  were optimized at the SR-CCSD(T) level. All the product species resulting from vertical electron detachments were similarly calculated at those geometries. We determined the first vertical detachment energy (VDE<sub>1</sub>) of  $\text{UCl}_6^{2-}$  at the SR-CCSD(T) level as the ground-state energy difference between  $\text{UCl}_6^{-}$  and  $\text{UCl}_6^{2-}$  both at the optimized ground-state geometry of  $\text{UCl}_6^{2-}$ . In the same way, the VDE<sub>1</sub> of  $\text{UCl}_6^{-}$  was determined at the SR-CCSD(T) level. To understand the ground and low-lying excited-states of  $\text{UCl}_6^{2-}$  of  $5f^1$  type, we performed SR-CASPT2 calculations with an active space of two electrons in the complete shell of the seven 5f orbitals as active space, denoted as CAS(2,7). Similar SR-CASPT2 calculations using “CAS(1,7)” were applied to all the  $5f^1$  states of  $\text{UCl}_6^{-}$ . Besides, the CCSD(T) and CR-EOM-CCSD(T) methods at the SR level were used to calculate the  $5f^1$  excited states of  $\text{UCl}_6^{-}$ .

We then determined the SO coupling effects of those species with configurations of  $\text{U-}5f^n$  ( $n = 1, 2$ ). The small SO effects by the Cl atoms, estimated as a few 0.01 eV, were neglected. SO coupling was accounted by a state-interacting method with SO pseudopotentials,<sup>55</sup> where the SO splittings

were determined as a perturbation to the SR state energies and calculated from CASSCF wavefunctions. The diagonal matrix elements were replaced by the individual CCSD(T) or CR-EOM-CCSD(T) or CASPT2 state energies at the SR level, which are denoted as CASSCF/CCSD(T)/SO or CASSCF/CR-EOM-CCSD(T)/SO or CASSCF/CASPT2/SO methods, respectively.<sup>25–27,56–60</sup> In the CASSCF/CR-EOM-CCSD(T)/SO calculation for  $\text{UCl}_6^-$ , the CCSD(T) ground-state energy and the CR-EOM-CCSD(T)  $5f^1$  excited state energies were used as diagonal matrix elements of the SO coupling matrix. That is, the vertical excitation energies of  $\text{UCl}_6^{2-}$  and  $\text{UCl}_6^-$  at the SO level were calculated with the so-called CASSCF/CAS(2,7)PT2/SO and CASSCF/CR-EOM-CCSD(T)/SO methods, respectively.

The SO effects on the ground-state energies of  $\text{UCl}_6^-$  and  $\text{UCl}_6^{2-}$  were calculated with the CAS(1,7)SCF/CR-EOM-CCSD(T)/SO and CASSCF/CAS(2,7)PT2/SO approaches, including all  $5f^1$  and  $5f^2$  states, respectively, at the SR-CCSD(T) ground state geometries of  $\text{UCl}_6^{q-}$ . The SO-corrected  $\text{VDE}_1$  of  $\text{UCl}_6^{2-}$  at the CCSD(T) level was obtained by adding the above SO corrections on the ground-state energies of  $\text{UCl}_6^-$  and  $\text{UCl}_6^{2-}$  to the SR-CCSD(T)  $\text{VDE}_1$  value of  $\text{UCl}_6^{2-}$ . Similarly, the SO-corrected  $\text{VDE}_1$  of  $\text{UCl}_6^-$  at the CCSD(T) level was estimated based on the SO correction on the ground-state energy of  $\text{UCl}_6^-$  from CAS(1,7)SCF/CR-EOM-CCSD(T)/SO calculations at the SR-CCSD(T) ground state geometry of  $\text{UCl}_6^-$ . It is worth mentioning that the ground-state energy of  $\text{UCl}_6$  is hardly affected by SO effects due to the closed-shell character.

Using the CASSCF/CASPT2/SO approach with the CAS(7,10) active space, we calculated the lowest ligand-to-metal charge transfer (LMCT) excited state of  $\text{UCl}_6^-$  at the CCSD(T) ground-state geometry of  $\text{UCl}_6^{2-}$ , corresponding to an electronic transition from the Cl- $1t_{1g}$  orbital to the U- $5f$  shell. The 10 active orbitals include the (Cl- $3p$ ) $1t_{1g}$ , and (U- $5f$ ) $1a_{2u}$ ,  $2t_{2u}$ , and  $3t_{1u}$  orbitals. SR-CASPT2 calculations were performed on the lowest 33 doublet and 33 quartet LMCT excited states of gerade symmetry in this active space. The SO-coupled LMCT state energies were obtained by the CASSCF/CAS(7,10)PT2/SO approach, and the lowest LMCT excitation energies were obtained by subtracting the SO-coupled ground-state energy of  $\text{UCl}_6^-$  from the CASSCF/CAS(1,7)PT2/SO results with the whole  $5f$  valence shell as active orbitals. In all the CASPT2 calculations, the ionization potential/electron affinity (IPEA) corrected zeroth-order Hamiltonian<sup>61</sup> was used with an IPEA shift of 0.25 a.u.

To understand the chemical bonding in  $\text{UCl}_6^{q-}$  ( $q = 0-2$ ), natural bond orbital analyses as developed by the Weinhold group were carried out. We performed NLMO (natural localized molecular orbital) and natural population analyses using the program NBO 5.0,<sup>62</sup> and covalency analyses with NRT (natural resonance theory) using NBO 6.0.<sup>63</sup> The electronic wavefunctions were obtained from single-point DFT/B3LYP<sup>43,44</sup> calculations using Gaussian 09<sup>64</sup> at the SR-DFT/PBE optimized geometries from ADF 2010.02 calculations. In the Gaussian 09 calculations, we used the same pseudopotentials for U and the same basis sets for U and Cl as in the MOLPRO calculations.

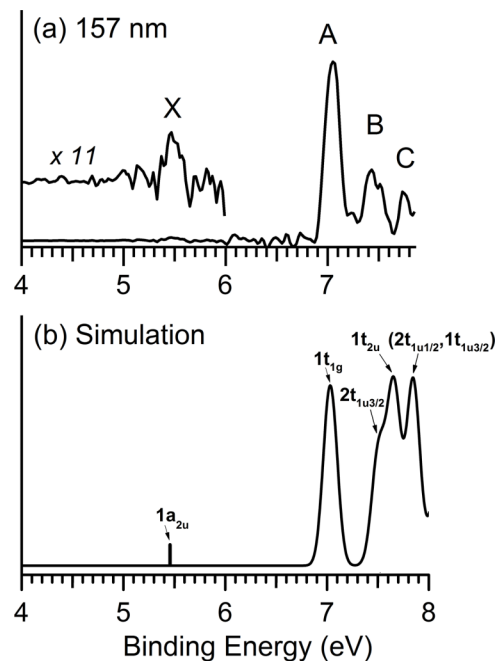


FIG. 1. (a) Photoelectron spectrum of  $\text{UCl}_6^-$  at 157 nm (7.866 eV) and 20 K. (b) The simulated spectrum at the relativistic DFT level, obtained by fitting each VDE with a Gaussian of 0.14 eV width except the weak  $1a_{2u}$  detachment channel.

### III. EXPERIMENTAL RESULTS

The photoelectron spectra of  $\text{UCl}_6^-$  and  $\text{UCl}_6^{2-}$  are shown in Figs. 1 and 2, respectively. All the observed VDEs for  $\text{UCl}_6^-$  and  $\text{UCl}_6^{2-}$  are given in Table I, where they are compared with the theoretical data. The transition from the ground state of  $\text{UCl}_6^-$  and  $\text{UCl}_6^{2-}$  to that of the corresponding final state is labeled as X and the letters (A, B, C, ...) designate detachment transitions to the excited states of the final state.

#### A. $\text{UCl}_6^-$

The photoelectron spectrum of  $\text{UCl}_6^-$  at 157 nm and 20 K is shown in Fig. 1(a). The simulated spectrum is shown in Fig. 1(b) for comparison and will be discussed later. Three intense bands (A, B, and C) are observed at very high binding energies, with VDEs of 7.04, 7.43, and 7.73 eV, respectively. Careful examination reveals an extremely weak band near 5.5 eV, labeled as X (see inset of Fig. 1(a)). This band is barely above the noise level and should correspond to electron detachment from the  $5f$  electron in  $\text{UCl}_6^-$ . The X band defines the EA for  $\text{UCl}_6$ . However, the extremely weak signal and poor signal-to-noise ratio of this band prevent us from measuring an accurate electron binding energy. The VDE is estimated to be  $5.5 \pm 0.1$  eV and the adiabatic detachment energy (ADE) or the EA of  $\text{UCl}_6$  is estimated to be  $5.3 \pm 0.2$  eV.

The extremely weak detachment cross section of the X band suggests that the highest singly occupied molecular orbital (SOMO) of  $\text{UCl}_6^-$  is mainly of  $5f_{xy}$  character, which was shown previously to give rise to very low detachment cross sections for  $\text{UF}_5^-$  and  $\text{UCl}_5^-$ .<sup>28,31</sup> The current observation for  $\text{UCl}_6^-$  confirms unequivocally why we were not able to obtain the PES spectrum of  $\text{UF}_6^-$  previously.<sup>28</sup> Without the strong

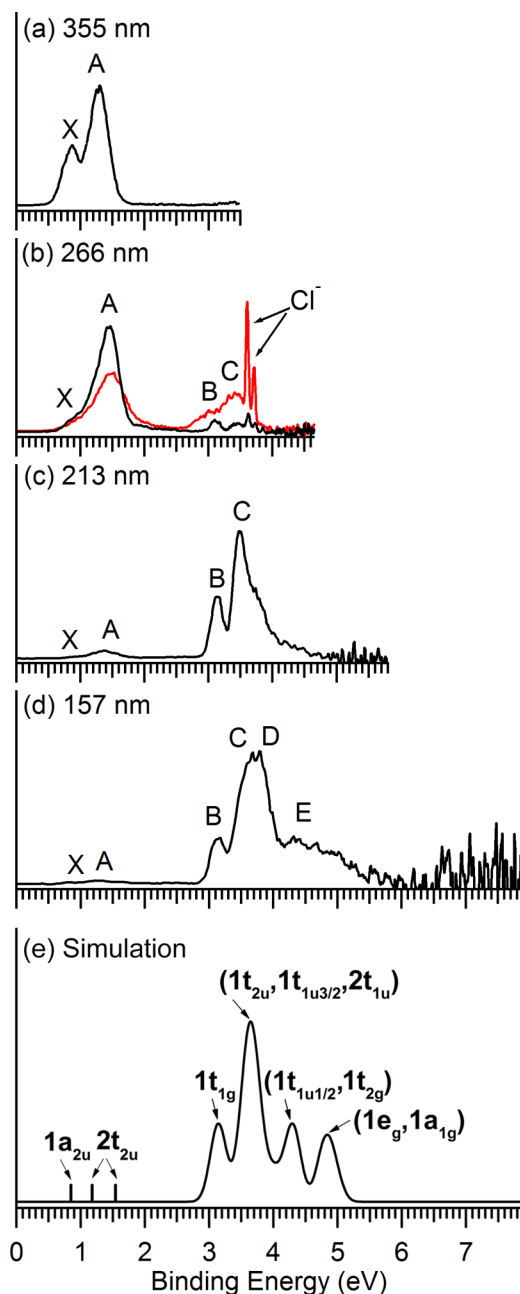


FIG. 2. Photoelectron spectra of  $\text{UCl}_6^{2-}$ . Experiment was done at 20 K with detachment wavelengths of (a) 355 nm (3.496 eV), (b) 266 nm (4.661 eV) (room temperature spectrum in red, showing stronger features due to  $\text{Cl}^-$ , see text), (c) 213 nm (5.821 eV), and (d) 157 nm (7.866 eV). (e) The simulated spectrum at the relativistic DFT level with CASSCF/CR-EOM-CCSD(T)/SO corrections by fitting each VDE with a Gaussian of 0.26 eV width except the weak  $1a_{2u}$  and  $2t_{2u}$  channels.

detachment features from the  $\text{Cl}3p$  orbitals at the high binding energy side, corresponding to bands A, B, and C (Fig. 1(a)), it would not be possible for us to observe the feeble detachment feature from the 5f SOMO of  $\text{UCl}_6^-$ . In fact, we tried to take the spectrum of  $\text{UCl}_6^-$  at 213 nm (5.821 eV) and were not able to observe any signals for the X band above the noise level. In the case of  $\text{UF}_6^-$ , the binding energies of the F2p orbitals were too high to be observed at 157 nm, the highest photon energy available, thwarting our opportunity to directly measure the EA of the important  $\text{UF}_6$  molecule.<sup>28</sup>

## B. $\text{UCl}_6^{2-}$

We were able to measure the photoelectron spectra of  $\text{UCl}_6^{2-}$  at 20 K and four different photon energies, as shown in Figs. 2(a)-2(d). We also obtained the 266 nm spectrum at room temperature (red curve in Fig. 2(b)) for comparison. The simulated spectrum is shown in Fig. 2(e) to be discussed later. At 355 nm (Fig. 2(a)), two bands (X and A) are resolved with VDEs of 0.86 and 1.5 eV, respectively. From the onset of the X band, we estimate an ADE of 0.60 eV, which should correspond to the EA of the  $\text{UCl}_6^-$  anion or the second EA of neutral  $\text{UCl}_6$ . The  $\text{UCl}_6$  molecule is among only a few species for which the second EAs have been measured. Band A is broad with strong signals ranging from 1.0 to 1.7 eV and even weaker signals around 2 eV (Fig. 2(b)). In fact, the higher binding energy side of band A is cut off by the repulsive Coulomb barrier (RCB) at 355 nm (*vide infra*). Following an energy gap, two weak features, B and C, are observed at 266 nm (Fig. 2(b)) and these two bands become the dominating features at higher photon energies. The weak signals of the B and C bands at 266 nm are due to electron tunneling through the RCB,<sup>65</sup> as will be discussed below. In addition, we observe two sharp peaks at 266 nm due to detachment from  $\text{Cl}^-$ , corresponding to binding energies at 3.613 and 3.722 eV for the  $^2P_{3/2}$  and  $^2P_{1/2}$  final states of Cl, respectively.<sup>66,67</sup> The  $\text{Cl}^-$  detachment features are significantly enhanced in the room temperature spectrum (red curve in Fig. 2(b)). Since the  $\text{Cl}^-$  signals are not observed in the higher photon energy spectra, they are likely derived from photodissociation of  $\text{UCl}_6^{2-}$  to  $\text{UCl}_5^- + \text{Cl}^-$  upon photoabsorption at 266 nm, followed by detachment from a second photon. The electron detachment energy of the  $\text{UCl}_5^-$  fragment is above 4.7 eV and cannot be observed at 266 nm (4.661 eV).<sup>31</sup>

The B and C bands are significantly enhanced at 213 nm (Fig. 2(c)), whereas the X and A bands become very weak. As will be shown below, the X and A bands are from detachment of 5f-based MOs, which have much lower detachment cross sections. A shoulder is observed on the higher binding energy side of band C at 213 nm, and it becomes a dominant band (D) at 157 nm (Fig. 2(d)). More features (E) are observed at higher binding energies in the 157 nm spectrum.

Comparing the spectrum at 213 nm (Fig. 2(c)) with that at 157 nm (Fig. 2(d)), one notes that band E is cut off in the lower photon energy spectrum and the relative intensity of band D is significantly reduced. This photon energy dependent spectral cutoff is a characteristic of PES of multiply charged anions and is a result of the RCB present universally for electron detachment from multiply charged anions.<sup>68</sup> From the 213 nm (5.821 eV) spectrum, we can see that the spectral cutoff is around 3.6 eV, which yields a RCB of  $\sim 2.2$  eV ( $h\nu - \text{cutoff}$ ). The RCB sets the minimum kinetic energy for photoelectrons to be emitted without tunnelling. The estimated RCB of 2.2 eV is consistent with the spectral cutoff at 157 nm (7.866 eV), where no signals are observed in the high binding energy side above 5.5 eV. Therefore, at 266 nm (4.661 eV), the B and C bands are below the RCB and the weak signals observed for the B and C bands are results of electron tunnelling through the RCB (Fig. 2(b)).<sup>65</sup> In fact, the relative intensity and shape of band A at 355 nm (Fig. 2(a)) are also affected by the RCB,

TABLE I. Observed VDEs of  $\text{UCl}_6^-$  and  $\text{UCl}_6^{2-}$  in comparison with calculated VDEs and the dominantly ionized MOs. All energies are in eV.

$\text{UCl}_6^-$			$\text{UCl}_6^{2-}$		
Expt.	TDDFT <sup>a</sup>	MO	Expt.	WFT <sup>b</sup> /DFT <sup>c</sup>	MO
X 5.5 (1)	5.44	1a <sub>2u-5/2</sub>	X 0.86(8)	0.85 <sup>d</sup>	1a <sub>2u-5/2</sub> <sup>e</sup>
			A ~ 1.5	{ 1.19 <sup>b</sup> 1.58 <sup>b</sup> 1.91 <sup>b</sup> 2.07 <sup>b</sup> }	{ 2t <sub>2u-3/2</sub> <sup>e</sup> 2t <sub>2u-5/2</sub> <sup>e</sup> 3t <sub>1u-3/2</sub> <sup>e</sup> 3t <sub>1u-1/2</sub> <sup>e</sup> }
A 7.04(8)	<b>7.00-7.07</b>	1t <sub>1g-3/2,1/2</sub>	B 3.14(8)	<b>3.10-3.19</b>	1t <sub>1g-3/2,1/2</sub>
B 7.43(8)	{ 7.47-7.53 7.61-7.70}	{ 2t <sub>1u-3/2</sub> 1t <sub>2u-5/2,3/2</sub> }	C 3.50(15)	{ 3.52-3.62 3.57-3.66}	{ 1t <sub>2u-5/2,3/2</sub> 1t <sub>1u-3/2</sub> }
C 7.73(8)	{ 7.84-7.84 7.82-7.90}	{ 2t <sub>1u-1/2</sub> 1t <sub>1u-3/2</sub> }	D 3.81(15)	3.70-3.78	2t <sub>1u-3/2,1/2</sub>
...	8.07-8.08	1t <sub>1u-1/2</sub>	E ~ 4.3	{ 4.00-4.00 4.24-4.35}	{ 1t <sub>1u-1/2</sub> 1t <sub>2g-5/2,3/2</sub> }
...	8.43-8.55	1t <sub>2g-5/2,3/2</sub>	Tail > 4.5	{ 4.74-4.84 4.93-4.96}	{ 1e <sub>g-3/2</sub> 1a <sub>1g-1/2</sub> }
...	{ 8.96-8.98 9.05-9.07}	{ 1a <sub>1g-1/2</sub> 1e <sub>g-3/2</sub> }			

<sup>a</sup>TDDFT of all SO-coupled states of  $\text{UCl}_6^-$  corresponding to dominantly one-electron detachment from  $\text{UCl}_6^-$ . The energy scale is shifted by  $-0.42$  eV to match the experimental peak A with the onset at  $7.00$  eV shown in bold face.

<sup>b</sup>The four VDEs corresponding to band A were calculated using WFT (CASSCF/CR-EOM-CCSD(T)/SO) as the energy difference between the ground state ( $E_{5/2u}$ ) and the four SO-coupled  $5f^1$  excited states of  $\text{UCl}_6^-$  (see Table V).

<sup>c</sup>The VDEs corresponding to detachment from ligand orbitals (band B and higher) are Kohn-Sham MO energies of  $\text{UCl}_6^{2-}$ , assuming that the correlation and reorganization errors are always the same in the Cl-3p shell. The energy scale is shifted by  $-0.21$  eV to match the experimental peak B with the onset at  $3.10$  eV shown in bold face. For the meaning of Kohn-Sham MO energies, see Ref. 96.

<sup>d</sup>Obtained by subtracting the theoretical energy difference  $2.25$  eV between the ground state and the first charge-transfer excited state (Cl-3p, 1t<sub>1g</sub> → U-5f) of  $\text{UCl}_6^-$  [according to CASSCF/CASPT2(7,10)/SO calculations] from the experimental  $3.1$  eV of the onset of the B band.

<sup>e</sup>Singly occupied MO of  $\text{UCl}_6^-$ .

resulting in the apparent high relative intensity of the X band compared with that in the 266 nm spectrum.

#### IV. THEORETICAL RESULTS

The calculated energies of the ground and excited states of  $\text{UCl}_6^{2-}$  and  $\text{UCl}_6^-$  using *ab initio* WFT methods at the SR and SO levels are given in Tables II–V. The first ADE and VDE of  $\text{UCl}_6^-$  and  $\text{UCl}_6^{2-}$ , calculated at the CCSD(T) level with SR and SO coupling corrections, are given in Table VI and compared with the experimental data. The theoretical VDEs of  $\text{UCl}_6^-$  and  $\text{UCl}_6^{2-}$  based on the combination of TDDFT and WFT calculations are presented in Tables SI and SII, respectively, and two different notations for the irreducible representations of double group  $O_h^*$  are listed in Table SIII of the supplementary material.<sup>69</sup> The optimized structural properties for all three uranium hexachlorides  $\text{UCl}_6^{q-}$  ( $q = 0-2$ ) at the SR-CCSD(T) level of theory are given in Table VII. The lowest vertical excitation energies ( $\Delta E$  in eV) from the U-5f type level in  $\text{UCl}_6^-$  by CASSCF/CR-EOM-CCSD(T)/SO calculations and in  $\text{UCl}_6^{2-}$  by CASSCF/CASPT2/SO calculations are reported in Table VIII and are compared with theoretical literature results<sup>9,70</sup> and experimental vertical absorption band values<sup>8,11,71–76</sup> measured in crystals or solutions.

##### A. The geometrical structures of $\text{UCl}_6^{q-}$ ( $q = 0-2$ )

All three molecules are found to have octahedral symmetry ( $O_h$ ), regardless of their charge states. Table VII shows

that upon filling electrons into the U-5f shell of  $\text{UCl}_6$ , the U–Cl bond lengths increase by 8 pm in  $\text{UCl}_6^-$  and by 21 pm in  $\text{UCl}_6^{2-}$  at the SR-CCSD(T) level, primarily as a result of the reduced effective charges on U and the increased intramolecular Coulomb repulsion in the anions. The trend of the calculated gas phase U–Cl bond lengths is consistent with the experimental values measured in the condensed phase.<sup>77–83</sup> In particular, for  $\text{UCl}_6^{2-}$ , the counterions in the crystal lattice counterbalance the strong Coulomb repulsion between the Cl<sup>-</sup> ions, resulting in shorter  $R(\text{U–Cl})$  values than in vacuum. The geometric and electronic structures are reasonably reproduced by the DFT approximation, which gives confidence in the calculated (harmonic) symmetric stretching vibrational frequencies. The frequencies agree within a few percent with the experimental values.<sup>84,85</sup> According to Badger's rule,<sup>86</sup> they correlate with the bond lengths, decreasing by 30 and 47  $\text{cm}^{-1}$ , respectively, from  $\text{UCl}_6$  to  $\text{UCl}_6^-$  to  $\text{UCl}_6^{2-}$ .

##### B. Molecular orbitals (MOs) of $\text{UCl}_6^{q-}$ ( $q = 0-2$ )

The one-electron MO schemes of  $\text{UCl}_6^{q-}$  ( $q = 0-2$ ), based on DFT calculations with SR and SO coupling, are displayed in Fig. 3, where the dominant atomic character of each MO is indicated. For  $O_h$  symmetry, the six Cl-3p $\sigma$  AOs give rise to MOs of a<sub>1g</sub>, e<sub>g</sub>, and t<sub>1u</sub> species; the twelve Cl-3p $\pi$  AOs give rise to MOs of t<sub>1g</sub>, t<sub>2g</sub>, t<sub>1u</sub>, and t<sub>2u</sub> species. The two sets of t<sub>1u</sub> MOs are  $\sigma$ - $\pi$  mixed. The dative Cl-3p bonding is due to mixing of the 1e<sub>g</sub>( $\sigma$ ) and 1t<sub>2g</sub>( $\pi$ ) ligand orbitals with the U-6d shell, and of the 1,2t<sub>1u</sub>( $\sigma\pi$ ) and 1t<sub>2u</sub>( $\pi$ ) ligand orbitals with the U-5f shell. Accordingly, the Cl-3p $\pi$ (1t<sub>1g</sub>) and the U-5f(1a<sub>2u</sub>)

TABLE II. Vertically excited singlet and triplet U-5f<sup>2</sup> type terms of UCl<sub>6</sub><sup>2-</sup> [from scalar-relativistic CAS(2,7)PT2 calculations] at the CCSD(T)-optimized <sup>3</sup>T<sub>1g</sub> (t<sub>2u</sub><sup>2</sup>) ground-state geometry: energies and O<sub>h</sub>-ligand-field split occupations of orbital-pairs.

Terms	Main contributions	$\Delta E/\text{eV}$	$\Delta\bar{\nu}/\text{cm}^{-1}$
X <sup>3</sup> T <sub>1g</sub>	45%t <sub>2u</sub> t <sub>2u</sub> + 35%t <sub>2u</sub> a <sub>2u</sub> + 19%t <sub>2u</sub> t <sub>1u</sub> + 1%t <sub>1u</sub> t <sub>1u</sub>	0.00	0
a <sup>3</sup> T <sub>2g</sub>	73%t <sub>1u</sub> a <sub>2u</sub> + 27%t <sub>2u</sub> t <sub>1u</sub>	0.16	1 309
a <sup>3</sup> T <sub>1g</sub>	42%t <sub>2u</sub> t <sub>2u</sub> + 23%t <sub>2u</sub> a <sub>2u</sub> + 19%t <sub>2u</sub> t <sub>1u</sub> + 16%t <sub>1u</sub> t <sub>1u</sub>	0.18	1 479
<sup>3</sup> E <sub>g</sub>	100%t <sub>2u</sub> t <sub>1u</sub>	0.26	2 082
b <sup>3</sup> T <sub>1g</sub>	62%t <sub>1u</sub> t <sub>1u</sub> + 20%t <sub>2u</sub> a <sub>2u</sub> + 11%t <sub>2u</sub> t <sub>2u</sub> + 7%t <sub>2u</sub> t <sub>1u</sub>	0.67	5 405
b <sup>3</sup> T <sub>2g</sub>	73%t <sub>1u</sub> t <sub>2u</sub> + 27%t <sub>1u</sub> a <sub>2u</sub>	0.67	5 440
<sup>3</sup> A <sub>2g</sub>	100%t <sub>2u</sub> t <sub>1u</sub>	0.77	6 172
a <sup>1</sup> T <sub>1g</sub>	58%t <sub>2u</sub> a <sub>2u</sub> + 42%t <sub>2u</sub> t <sub>1u</sub>	0.65	5 268
a <sup>1</sup> E <sub>g</sub>	85%t <sub>2u</sub> <sup>2</sup> + 7%t <sub>1u</sub> <sup>2</sup> + 8%t <sub>2u</sub> t <sub>1u</sub>	0.66	5 285
a <sup>1</sup> A <sub>1g</sub>	71%a <sub>2u</sub> <sup>2</sup> + 28%t <sub>1u</sub> <sup>2</sup>	0.70	5 609
a <sup>1</sup> T <sub>2g</sub>	36%t <sub>2u</sub> t <sub>1u</sub> + 49%t <sub>1u</sub> t <sub>1u</sub> + 9%t <sub>2u</sub> t <sub>2u</sub> + 6%t <sub>1u</sub> a <sub>2u</sub>	0.85	6 852
b <sup>1</sup> T <sub>2g</sub>	56%t <sub>2u</sub> t <sub>2u</sub> + 43%t <sub>1u</sub> a <sub>2u</sub>	1.73	13 990
b <sup>1</sup> E <sub>g</sub>	89%t <sub>2u</sub> t <sub>1u</sub> + 7%t <sub>1u</sub> <sup>2</sup> + 4%t <sub>2u</sub> <sup>2</sup>	1.99	16 030
b <sup>1</sup> A <sub>1g</sub>	59%t <sub>2u</sub> <sup>2</sup> + 23%t <sub>1u</sub> <sup>2</sup> + 18%a <sub>2u</sub> <sup>2</sup>	2.30	18 550
b <sup>1</sup> T <sub>1g</sub>	58%t <sub>1u</sub> t <sub>2u</sub> + 42%t <sub>2u</sub> a <sub>2u</sub>	2.33	18 759
c <sup>1</sup> T <sub>2g</sub>	51%t <sub>1u</sub> a <sub>2u</sub> + 34%t <sub>2u</sub> t <sub>2u</sub> + 11%t <sub>1u</sub> t <sub>2u</sub> + 5%t <sub>1u</sub> t <sub>1u</sub>	2.37	19 106
c <sup>3</sup> T <sub>1g</sub>	55%t <sub>2u</sub> t <sub>1u</sub> + 21%t <sub>1u</sub> t <sub>1u</sub> + 21%t <sub>2u</sub> a <sub>2u</sub> + 2%t <sub>2u</sub> t <sub>2u</sub>	2.46	19 854
a <sup>1</sup> A <sub>2g</sub>	100%t <sub>2u</sub> t <sub>1u</sub>	2.50	20 125
d <sup>1</sup> T <sub>2g</sub>	52%t <sub>1u</sub> a <sub>2u</sub> + 46%t <sub>1u</sub> t <sub>1u</sub> + 2%t <sub>2u</sub> t <sub>2u</sub>	2.66	21 490
c <sup>1</sup> E <sub>g</sub>	86%t <sub>1u</sub> <sup>2</sup> + 10%t <sub>2u</sub> <sup>2</sup> + 2%t <sub>2u</sub> t <sub>1u</sub>	2.70	21 739
c <sup>1</sup> A <sub>1g</sub>	49%t <sub>1u</sub> <sup>2</sup> + 39%t <sub>2u</sub> <sup>2</sup> + 12%a <sub>2u</sub> <sup>2</sup>	4.93	39 799

type MOs are non-bonding and form the HOMO and LUMO of UCl<sub>6</sub> (Figs. 3 and 4). One t<sub>1u</sub> MO is Cl-3p/U-6p anti-bonding and is significantly SO-split. The other occupied t<sub>1u</sub> MO and the t<sub>2u</sub> MO of Cl-3p type have only weak covalent character. The higher empty 3t<sub>1u</sub> and 2t<sub>2u</sub> U-5f type MOs are weakly antibonding and are also subject to notable SO-splitting.

The occupied valence MOs of UCl<sub>6</sub> are all derived from the Cl 3p atomic orbitals (AO), whereas the U-5f shell is just singly or doubly occupied in the two anions. The 5f shell of 7 degenerate orbitals spans the a<sub>2u</sub> (f<sub>x</sub>y<sub>z</sub>), t<sub>2u</sub> (f<sub>xz</sub><sup>2</sup>, f<sub>yz</sub><sup>2</sup>, f<sub>z</sub>(x<sup>2</sup>-y<sup>2</sup>)), and t<sub>1u</sub> (f<sub>x</sub><sup>3</sup>, f<sub>y</sub><sup>3</sup>, f<sub>z</sub><sup>3</sup>) MOs in O<sub>h</sub> symmetry. The Cl<sup>-</sup> ligands form dominantly ionic interactions with the central U<sup>n+</sup> cation, as well as dative bonds into the U-5f6d shell. The 1t<sub>1g</sub> orbital, mainly of nonbonding Cl-3pπ character, is the HOMO of UCl<sub>6</sub><sup>0</sup>. The LUMO of UCl<sub>6</sub><sup>0</sup> is the 1a<sub>2u</sub> orbital of U-5f character.

The extra electron in UCl<sub>6</sub><sup>-</sup> enters the LUMO to give the 1a<sub>2u</sub> SOMO. In UCl<sub>6</sub><sup>2-</sup> at the single-determinant DFT level,

the two extra electrons enter the U-5f 2t<sub>2u</sub> shell (DOMO) to give a triplet spin state for the dianion. We note that at the restricted open-shell multiconfigurational SCF level, the atomic LS states of f<sup>2</sup> character are single configuration states of single- or multi-determinantal type with various occupied f-AO pairs, becoming multi-configurational in the ligand-field split space of O<sub>h</sub>-symmetry adapted orbitals.

Evidently, significant *orbital mixing* of the 5f-based 1a<sub>2u</sub>, 2t<sub>2u</sub>, and 3t<sub>1u</sub> MOs occurs upon SO coupling, which splits the 1a<sub>2u</sub>, 2t<sub>2u</sub>, and 3t<sub>1u</sub> orbitals into e<sub>5/2u</sub>, u<sub>3/2u</sub> + e<sub>5/2u</sub>, and u<sub>3/2u</sub> + e<sub>1/2u</sub> spinors, respectively, in O<sub>h</sub><sup>\*</sup> double-group representations. Due to second-order SO coupling, the two e<sub>5/2u</sub> spinors from 2t<sub>2u</sub> and 1a<sub>2u</sub> can mix, so can the two u<sub>3/2u</sub> spinors from 2t<sub>2u</sub>, and 3t<sub>1u</sub>. Accordingly, with SO coupling, the ground-state electron configurations of UCl<sub>6</sub><sup>-</sup> and UCl<sub>6</sub><sup>2-</sup> are virtually (a<sub>2u</sub>t<sub>2u</sub>)<sup>n</sup> (n = 1, 2) with slight mixing with the energetically separated t<sub>1u</sub> orbitals. This orbital mixing causes a breakdown of Koopmans' theorem and considerable

TABLE III. The lowest seven SO-coupled states of UCl<sub>6</sub><sup>2-</sup> (from CASSCF/CAS(2,7)PT2/SO calculations) at the geometry of <sup>3</sup>T<sub>1g</sub> (5f-t<sub>2u</sub><sup>2</sup>) as optimized by SR-CCSD(T). SO-mixing of LS-U-5f<sup>2</sup> type O<sub>h</sub>-ligand-field configuration states. The SR leading term of each SO-coupled state is in boldface.

SO level	Main contributions	$\Delta E/\text{eV}$	$\Delta\bar{\nu}/\text{cm}^{-1}$
XA <sub>1g</sub>	93% <b>X<sup>3</sup>T<sub>1g</sub></b> + 7%a <sup>1</sup> A <sub>1g</sub>	0	0
aT <sub>1g</sub>	51% <b>X<sup>3</sup>T<sub>1g</sub></b> + 31%a <sup>3</sup> T <sub>2g</sub> + 9% <sup>3</sup> E <sub>g</sub> + 8%a <sup>1</sup> T <sub>1g</sub>	0.09	696
aE <sub>g</sub>	50% <b>a<sup>3</sup>T<sub>2g</sub></b> + 26%a <sup>3</sup> T <sub>1g</sub> + 10%a <sup>1</sup> E <sub>g</sub> + 14% <b>X<sup>3</sup>T<sub>1g</sub></b>	0.14	1107
aT <sub>2g</sub>	53% <b>a<sup>3</sup>T<sub>1g</sub></b> + 33% <sup>3</sup> E <sub>g</sub> + 7%a <sup>1</sup> T <sub>2g</sub>	0.24	1907
bT <sub>1g</sub>	46% <b>X<sup>3</sup>T<sub>1g</sub></b> + 46%a <sup>3</sup> T <sub>2g</sub> + 7% <sup>3</sup> E <sub>g</sub>	0.66	5340
bE <sub>g</sub>	56% <b>a<sup>3</sup>T<sub>1g</sub></b> + 8%a <sup>3</sup> T <sub>2g</sub> + 14% <b>X<sup>3</sup>T<sub>1g</sub></b> + 8%b <sup>3</sup> T <sub>1g</sub> + 2%b <sup>1</sup> E <sub>g</sub>	0.66	5350
bT <sub>2g</sub>	39% <b>X<sup>3</sup>T<sub>1g</sub></b> + 29%a <sup>3</sup> T <sub>2g</sub> + 14%a <sup>3</sup> T <sub>1g</sub> + 9% <sup>3</sup> E <sub>g</sub> + 1%b <sup>1</sup> T <sub>2g</sub>	0.67	5367

TABLE IV. The three scalar relativistic  $5f^1$  terms of  $\text{UCl}_6^-$  from CR-EOM-CCSD(T) and CCSD(T) and CAS(1,7)PT2 calculations, at the CCSD(T)-optimized geometry of  ${}^3T_{1g}(t_{2u}^2)$  of  $\text{UCl}_6^{2-}$  (U–Cl bond length of 2.669 Å).

Terms <sup>a</sup>	CR-EOM-CCSD(T)	CCSD(T)	CASPT2
	$\Delta E/\text{eV}$	$\Delta E/\text{eV}$	$\Delta E/\text{eV}$
${}^2A_{2u}$	0	0	0
${}^2T_{2u}$	0.25	0.28	0.28
${}^2T_{1u}$	0.65	0.69	0.76

<sup>a</sup>In the CR-EOM-CCSD(T) and CCSD(T) calculations,  $D_{2h}$  symmetry is used for electronic wavefunction. Therefore, the degenerate states  ${}^2T_{2u}$  and  ${}^2T_{1u}$  in  $O_h$  symmetry were calculated as states  $a^2B_{1u}$  and  $b^2B_{1u}$  in  $D_{2h}$  symmetry, with equivalent results for  $i = 1, 2, 3$ .

complexity in the PES spectra of the dianion, as will be discussed below. In Fig. 3, the  $1t_{1g}$  Cl-3p HOMO is used as the zero energy reference for all three  $\text{UCl}_6^{q-}$  species. The common approximate exchange-correlation functionals are known to incorrectly reproduce the electron repulsion in compact orbital shells; therefore, the upper U-5f type MO levels of  $\text{UCl}_6^{2-}$  are predicted more than 0.5 eV too high by DFT.

The three-dimensional MO contour pictures of  $\text{UCl}_6^{q-}$  are shown in Fig. 4, where the occupation and bonding character for  $\text{UCl}_6^-$  are given. It should be noted that the shapes of the  $1t_{1u}$  and  $2t_{1u}$  orbitals are interchanged from  $\text{UCl}_6$  to  $\text{UCl}_6^{2-}$ .

### C. The ground electronic states of $\text{UCl}_6^{q-}$ ( $q = 0-2$ )

In  $\text{UCl}_6^0$ , U is in its highest oxidation state of +6 with a  $5f^0$  singlet ground state ( ${}^1A_{1g}$ ). The  $\text{UCl}_6^-$  anion has a doublet ground state ( ${}^2A_{2u}$ ) with one 5f electron in the  $1a_{2u}$  MO (Fig. 3). The  $\text{UCl}_6^{2-}$  dianion has two electrons, resulting in more complicated electronic structures due to strong Fermi, Coulomb, and SO correlation effects between the U-5f electrons. The states and energies derived for different spin and LS couplings and owing to mixing of different octahedral orbital configurations are given in Table II. At the SR-DFT level, the electronic ground term of  $\text{UCl}_6^{2-}$  is a degenerate  ${}^3T_{1g}$  one with the two electrons occupying the  $2t_{2u}$  U-5f shell at  $O_h$  symmetry (Fig. 3). This state should be subject to static or dynamic Jahn-Teller distortion of the octahedral symmetry. The  ${}^3T_{1g}(2t_{2u}^2)$  ground term also dominates the CAS wavefunction, but contributes only 45%, with  $2t_{2u}^11a_{2u}^1$  and  $2t_{2u}^13t_{1u}^1$  configurations contributing 35% and 19%,

TABLE V. The five SO-coupled levels arising from the  $5f^1$  configuration of  $\text{UCl}_6^-$ , from CASSCF/CR-EOM-CCSD(T)/SO calculations, at the CCSD(T)-optimized geometry of  ${}^3T_{1g}(t_{2u}^2)$  of  $\text{UCl}_6^{2-}$  (U–Cl bond length 2.669 Å).

SO levels	Main contributions <sup>a</sup>	$\Delta E/\text{eV}$	$\Delta E_{\text{ref}}/\text{eV}^b$
$\text{XE}_{5/2u}$	$61\%{}^2A_{2u} + 39\%{}^2T_{2u}$	0.00	0.85
$\text{aU}_{3/2u}$	$66\%{}^2T_{2u} + 34\%{}^2T_{1u}$	0.34	1.19
$\text{aE}_{5/2u}$	$61\%{}^2T_{2u} + 39\%{}^2A_{2u}$	0.73	1.58
$\text{bU}_{3/2u}$	<b><math>66\%{}^2T_{1u} + 34\%{}^2T_{2u}</math></b>	1.06	1.91
$\text{aE}_{1/2u}$	<b><math>100\%{}^2T_{1u}</math></b>	1.22	2.07

<sup>a</sup>States with significant  ${}^2T_{1u}$  character of  $(3t_{1u})^1$  configuration marked in boldface should have low intensity in PES (see Table I and Fig. 5).

<sup>b</sup>The energies refer to the first calculated VDE of peak X (see footnote b in Table I).

TABLE VI. Observed and calculated ADEs and VDEs of the first detachment channel of  $\text{UCl}_6^-$  and  $\text{UCl}_6^{2-}$ . All energies are in eV.

		Expt. <sup>a</sup>	CCSD(T)	
			SO <sup>b</sup>	SR
$\text{UCl}_6^-$	ADE	5.3 (2)	5.53	5.26
	VDE	5.5 (1)	5.86	5.59
$\text{UCl}_6^{2-}$	ADE	0.60 (9)	0.46	0.09
	VDE	0.86 (8)	1.06	0.69

<sup>a</sup>The numbers in parentheses represent the experimental uncertainties in the last digit.

<sup>b</sup>The SO results for the VDE are obtained by combining the CASSCF/CASPT2/SO and CASSCF/CR-EOM-CCSD(T)/SO calculations (see Sec. II B); the SO results for the ADE are obtained using the SO corrections for the VDE values.

respectively. It must be noted, however, that all atomic LS- $f^2$  terms are of open-shell single-configuration multi-determinant type with symmetry-fixed rational mixing coefficients. The ligand-field splitting of the U-5f shell in the  $\text{UCl}_6$  species into  $a_{2u}$ ,  $t_{2u}$ , and  $t_{1u}$  by around  $\pm 0.5$  eV transforms these atomic single-configuration multi-determinant  $f^2$  functions into  $(a_{2u}, t_{1u}, t_{2u})^2$  multi-configuration functions with nearly rational mixing coefficients. With SO coupling, the electronic ground state of  $\text{UCl}_6^{2-}$  becomes a first-order Jahn-Teller non-active  $A_{1g}$  state (Table III), thus rendering the regular octahedral structure of the dianion. The strongly pseudo-configuration-mixed  ${}^3T_{1g}$  state contributes 93% to the SO-coupled  $A_{1g}$  state, while the remaining 7% come from  $1a_{2u}^2$  and  $3t_{1u}^2$  configurations (for details, see Tables II and III). Our calculated SO-coupled excitation energies of  $\text{UCl}_6^-$  at the SR-CCSD(T) ground-state geometry of  $\text{UCl}_6^{2-}$  are listed in Table V, and the higher VDEs of  $\text{UCl}_6^{2-}$  due to 5f electron detachment are obtained by reference to the first calculated VDE of peak X.

## V. THE CALCULATED ELECTRON BINDING ENERGIES AND INTERPRETATION OF THE OBSERVED PHOTOELECTRON SPECTRA

To interpret the PES spectra of  $\text{UCl}_6^-$  and  $\text{UCl}_6^{2-}$ , we calculated the electron binding energies and simulated the PES spectra based on the calculated VDEs. Several electronic states were calculated at a high level of correlated, quasi-relativistic SO-coupled theory. The calculated first ADE and VDE for  $\text{UCl}_6^-$  and  $\text{UCl}_6^{2-}$  are compared with the experimental values in Table VI. The theoretical results with SO corrections agree within about 0.3 eV of the experimental values. The calculated EA for  $\text{UCl}_6$  at both SO-CCSD(T) (5.53 eV) and SR-CCSD(T) (5.26 eV) levels agrees with the observed value ( $5.3 \pm 0.2$  eV) within the large experimental uncertainty. We recently calculated an EA of 5.20 eV at the SR-CCSD(T) level for  $\text{UF}_6$ ,<sup>28</sup> even though we were not able to measure the photoelectron spectrum of  $\text{UF}_6^-$ . The current study suggests that the previous theoretical EA for  $\text{UF}_6$  is reasonable.

### A. $\text{UCl}_6^-$

Electron detachment from the doublet ground state of  $\text{UCl}_6^-$  yields singlet and triplet final states of  $\text{UCl}_6^0$ . The

TABLE VII. Geometric symmetry, electronic ground state with the leading configuration, bond lengths ( $R(\text{U}-\text{Cl})$  in pm), and symmetric stretching vibrational frequencies ( $\nu_s(\text{U}-\text{Cl})$  in  $\text{cm}^{-1}$ ) calculated for  $\text{UCl}_6$ ,  $\text{UCl}_6^-$ , and  $\text{UCl}_6^{2-}$  in vacuum at the SR-CCSD(T) and SR-DFT levels, and experimental bond lengths in the crystal phase.

	SR-CCSD(T)		Expt. <sup>a</sup>	SR-DFT(PBE)		Expt. <sup>b</sup>	
	Symmetry	Ground state	$R(\text{U}-\text{Cl})$	$R(\text{U}-\text{Cl})$	$R(\text{U}-\text{Cl})$	$\nu_s(\text{U}-\text{Cl})^c$	$\nu_s(\text{U}-\text{Cl})$
$\text{UCl}_6$	$O_h$	$^1A_{1g}(f^0)$	245.4	241-251	247.1	347	367
$\text{UCl}_6^-$	$O_h$	$^2A_{2u}(f^1-1a_{2u})$	253.7	247,252,256	254.6	317	~344
$\text{UCl}_6^{2-}$	$O_h$	$^3T_{1g}(f^2-2t_{2u}^2)^d$	266.9	258-264	266.9	270	~302

<sup>a</sup>References 77–83.

<sup>b</sup>References 84 and 85.

<sup>c</sup>Harmonic approximation.

<sup>d</sup>The  $2t_{2u}^2$  configuration contributes only 45% to the  $f^2$  manifold; the  $^3T_{1g}$  LS-state contributes 93% to the SO coupled ground state (Tables II and III). In the CCSD(T) calculations, the Abelian  $D_{2h}$  subgroup symmetry is used for electronic wavefunctions. The degenerate state  $^3T_{1g}(f^2-2t_{2u}^2)$  in  $O_h$  symmetry was calculated as a  $^3B_{1g}(1b_{1u}1b_{k_u})$  state in  $D_{2h}$  symmetry, i, j, k = 1, 2, 3.

VDEs were computed as excitations from the singlet ground state of  $\text{UCl}_6$  to its singlet and triplet excited states using TDDFT at both the SAOP and B3LYP levels (Table SI).<sup>69</sup> The two levels of theory yielded similar VDEs; the values from the SAOP level are compared with the experimental data in Table I and are used to produce the simulated PES spectra for  $\text{UCl}_6^-$  in Fig. 1(b). The simulated spectrum was obtained by representing the calculated VDEs for each Cl-3p MO detachment by a unit Gaussian of width 0.14 eV. The detachment features from the much more compact, and therefore much weaker U-5f type MOs are simply indicated by short bars in Fig. 1(b). The qualitative similarity of the simulated and observed PES spectrum for  $\text{UCl}_6^-$  lends considerable confidence for the reliability of the spectral assignments.

As shown in Fig. 1(b) and Table I, the observed four bands X, A, B, and C correspond to one-electron detachments from orbitals or spinors of the following types: X from U-5f( $1a_{2u-5/2}$ ), A from SO-components Cl-3p( $1t_{1g-3/2,1/2}$ ), B from SO-components Cl-3p( $2t_{1u-3/2}$ ) and Cl-3p( $1t_{2u-5/2,3/2}$ ), and C from Cl-3p( $2t_{1u-1/2}$ ) and Cl-3p( $1t_{1u-3/2}$ ). The detachment energy of the SO-component of Cl-3p( $1t_{1u-1/2}$ ) is already above the 157 nm excitation photon energy limit (7.866 eV). The SOMO of  $\text{UCl}_6^-$  ( $5f_{xy^2-1a_{2u}}$ ) is comparably compact (Fig. 4), which explains why the detachment cross section of the X band is so weak in agreement with our previous experiment for  $\text{UF}_5^-$  and  $\text{UF}_6^-$ .<sup>28</sup>

## B. $\text{UCl}_6^{2-}$

Without SO coupling, electron detachment from the  $\text{UCl}_6^{2-}$  triplet ground state can result in doublet and quartet final states of  $\text{UCl}_6^-$ . Similar to the strong correlation effects observed in the electron detachment from  $\text{U}(f^3)\text{O}_2^-$ ,<sup>87</sup> the electron detachment from  $\text{U}(f^2)\text{Cl}_6^{2-}$  is also complicated by the interplay of strong SO coupling and multi-configurational electron correlations. The detachment channels are schematically illustrated in Fig. 5. The computed VDEs are given in Table SII<sup>69</sup> and compared with the experimental data in Table I and the simulated spectrum in Fig. 2(e). The simulated spectrum for  $\text{UCl}_6^{2-}$  was obtained by representing the calculated VDEs of each Cl-3p MO detachment feature by a unit Gaussian of width 0.28 eV. The detachment features of the much weaker U-5f type MOs are indicated by short bars in Fig. 2(e). The good agreement between the simulated and observed PES spectra for  $\text{UCl}_6^{2-}$  again confirms the reliability of the spectral assignments.

As shown in Table II, the leading configuration of the ground state of  $\text{UCl}_6^{2-}$  ( $^3T_{1g}$ ) is  $2t_{2u}^2$  (45%). Single electron detachment from this orbital should only result in two detachment channels with the final state configurations of  $2t_{2u-3/2}^1$  and  $2t_{2u-5/2}^1$ , corresponding to VDE<sub>2</sub> and VDE<sub>3</sub> in Fig. 5. However, the  $^3T_{1g}$  ground state of  $\text{UCl}_6^{2-}$  also consists of 35%  $2t_{2u}^11a_{2u}^1$  and 19%  $2t_{2u}^13t_{1u}^1$ , which lead to final state configurations of  $1a_{2u}^1$  (VDE<sub>1</sub>) and  $3t_{1u}^1$  (VDE<sub>4</sub>

TABLE VIII. The lowest vertical excitation energies ( $\Delta E$  in eV) within the U-5f shell of  $\text{UCl}_6^-$ , from CASSCF/CR-EOM-CCSD(T)/SO, and of  $\text{UCl}_6^{2-}$  from CASSCF/CASPT2/SO<sup>a</sup> calculations, at the SR-CCSD(T) optimized ground-state geometries with  $R(\text{U}-\text{Cl})$  bond lengths of 2.537 and 2.669 Å, respectively, in the gas phase, and comparison with reported theoretical results and experimental vertical absorption bands measured in crystals or solutions.

Anion	Level	$\text{XE}_{5/2u}$	$\text{aU}_{3/2u}$	$\text{aE}_{5/2u}$	$\text{bU}_{3/2u}$	$\text{aE}_{1/2u}$		
$\text{UCl}_6^-$	$\Delta E$	-0-	0.39	0.73	1.13	1.30		
	$E_{\text{calc}}^b$	-0-	0.34-0.47	0.84-0.91	1.16-1.39	1.33-1.54		
	$E_{\text{expt.}}^c$	-0-	~0.5	~0.85	~1.2	~1.45		
Dianion $\text{UCl}_6^{2-}$	Level	$\text{XA}_{1g}$	$\text{aT}_{1g}$	$\text{aE}_g$	$\text{aT}_{2g}$	$\text{bT}_{1g}$	$\text{bE}_g$	$\text{bT}_{2g}$
	$\Delta E$	-0-	0.09	0.14	0.24	0.66	0.66	0.67
	$E_{\text{expt.}}^d$	-0-	0.11,0.12	0.16	0.30	0.79, 0.84	0.63, 0.69	0.61

<sup>a</sup>Active space of 2-electrons in 7-orbitals, CAS(2,7).

<sup>b</sup>From SO-CASSCF and SO-CASPT2 calculations in Refs. 9 and 70.

<sup>c</sup>From Refs. 8, 11, and 71.

<sup>d</sup>From Refs. 72–76.

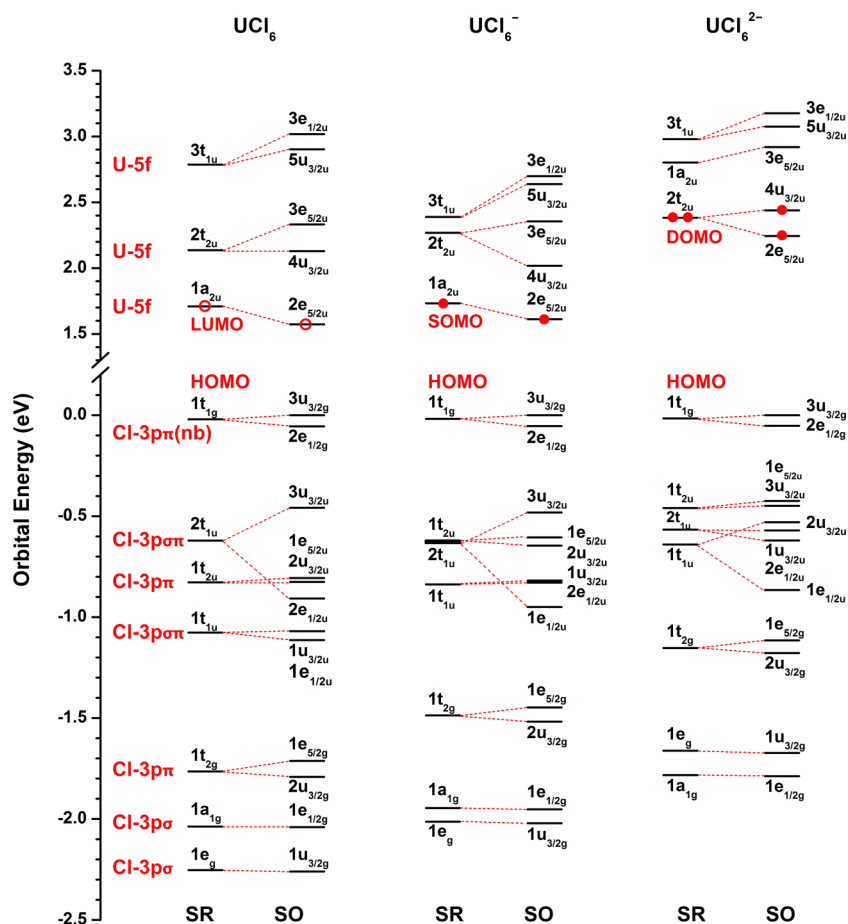


FIG. 3. SR and SO-coupled energies of the valence orbitals of  $\text{UCl}_6^{q-}$  ( $q = 0-2$ ) from relativistic DFT/PBE calculations (nb, nonbonding).

and  $\text{VDE}_5$ ). These detachments' transitions can be viewed as two-electron processes, which are direct manifestation of the strong electron correlation (or open-shell determinantal mixing) effects of the two 5f electrons in  $\text{UCl}_6^{2-}$ , thus leading to the breakdown of Koopmans' single-determinantal theorem. The intensities of these transitions are expected to be low, especially for the  $\text{VDE}_4$  and  $\text{VDE}_5$  channels, due to the low percentage of the  $2t_{2u}^1 3t_{1u}^1$  configuration (19%). As assigned in Table I, the  $\text{VDE}_1$  corresponding to  $\text{U}5f(1a_{2u-5/2})$  is assigned to the observed X band. The two detachment

channels leading to  $\text{U}5f(2t_{2u-5/2,3/2})$  should correspond to the more intense broad band A. The two channels leading to  $\text{U}5f(3t_{1u-3/2,1/2})$  should have very low relative intensities and should correspond to very weak signals on the higher binding energy side of band A ( $\text{VDE}_4$  and  $\text{VDE}_5$  in Fig. 5, but not shown in Fig. 2(e)). The strong band B then corresponds to one-electron detachment from  $\text{Cl}3p(1t_{1g-3/2,1/2})$ . The higher binding energy detachment bands (C, D, and E) are assigned to higher Cl-3p based ligand orbitals (Table I and Fig. 2(e)).

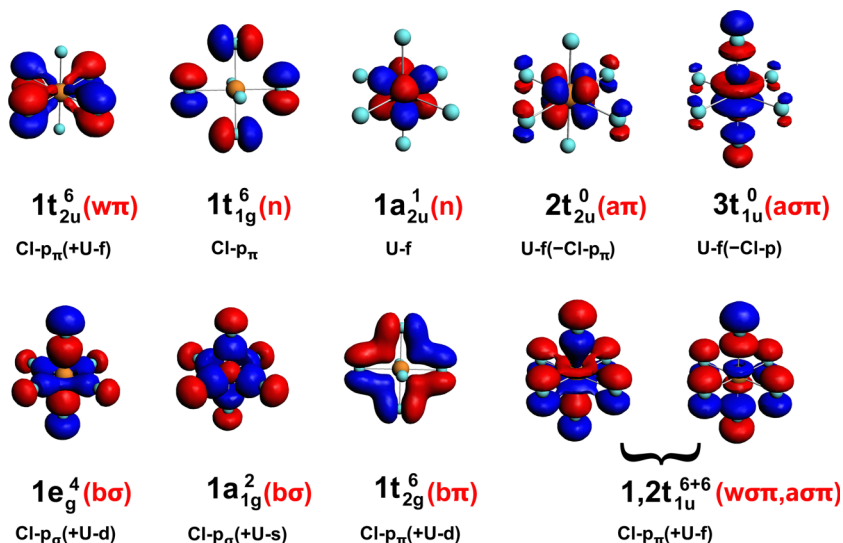


FIG. 4. Pictures of the relevant valence orbitals of  $\text{UCl}_6^-$  from DFT calculations and the orbital characters (b, bonding; w, weakly bonding; n, nonbonding; a, antibonding).

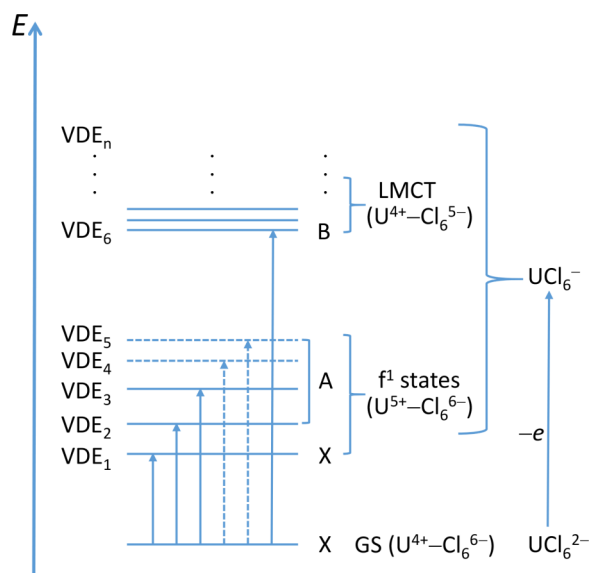


FIG. 5. Schematic illustration of the photodetachment processes from  $\text{UCl}_6^{2-}$ , and the detachment channels of VDE<sub>4</sub> and VDE<sub>5</sub> have low intensity in PES and are marked by a dotted line.

One of the two  $t_{1u}$  MOs has some anti-bonding contribution from the strongly SO-affected U-6p<sup>6</sup> core shell and is thus significantly SO-split due to the large SO splitting constant of U-6p (Figs. 3 and 4). The two SO components correspond to  $t_{1u-1/2}$  and  $t_{1u-3/2}$  ( $e_{1/2u}$  and  $u_{3/2u}$  in double-group representation, Fig. 3). The softness of the outer noble-gas core shells is well known for the bottom rows of the periodic table,<sup>25-27,31,88,89</sup> where the heavy noble-gas shells have an influence on the valency of the heavy metal atoms from the s- and early f-blocks. Without accounting for the SO splitting of the Cl-3p  $t_{1u}$  MOs of 0.4 eV, the spectral simulations would become visibly worse for both  $\text{UCl}_6^-$  and  $\text{UCl}_6^{2-}$ , indicating the valence participation of the Rn-6p noble-gas shell.

## VI. DISCUSSION

### A. The origin of the PES band widths

The experimental PES bands are all quite broad (Figs. 1 and 2), as a result of both overlapping detachment transitions, and extended Franck-Condon envelopes due to the geometry changes upon electron detachment (Table VII). These geometry changes result mainly from changes in the ionic interactions: the Coulomb attraction of formal ( $\text{U}^{5+}$ ) ( $\text{Cl}^{-1}$ )<sub>6</sub> in  $\text{UCl}_6^-$  is increased to ( $\text{U}^{6+}$ ) ( $\text{Cl}^{-1}$ )<sub>6</sub> upon U-5f( $1a_{2u}$ ) electron detachment (X band in Fig. 1). It is similarly decreased to ( $\text{U}^{5+}$ ) ( $\text{Cl}^{-5/6}$ )<sub>6</sub> upon detachment from the Cl-3p type MOs. The changes in ionic interactions upon detachment from  $\text{UCl}_6^{2-}$  are similar. In addition, there are larger SO and electron correlation effects. The instrumental resolution is much smaller, as indicated by the PES features of  $\text{Cl}^-$  in Fig. 2(b). The band widths of our low temperature PES spectra without thermal broadening are around 0.1–0.15 eV for the spectrum of  $\text{UCl}_6^-$  (Fig. 1) and 0.25–0.30 eV for  $\text{UCl}_6^{2-}$  (Fig. 2). The energy difference between the observed first ADE and VDE of  $\text{UCl}_6^{2-}$  is  $\sim 0.26$  eV, which should

be roughly the width of band X. The calculated harmonic U–Cl stretching vibrational frequencies of  $\text{UCl}_6^-$  and  $\text{UCl}_6$  are around 330  $\text{cm}^{-1}$  (Table VII), suggesting Huang-Rhys factors of  $S = \Delta E/h\nu_s \approx 7$  and 4, respectively, for  $\text{UCl}_6^-$  and  $\text{UCl}_6$ , with  $\Delta E = 0.26$  and 0.15 eV (i.e., the experimental and theoretical PES band widths). These relations follow from the theory of bond-length-change  $\Delta R$ /vibrational-band-width of highly symmetric molecules  $\text{AX}_n$  upon electronic excitation,<sup>90</sup>

$$\Delta R = 821 \times [S/(w\nu_s M_X)]^{1/2}, \quad (1)$$

where  $\Delta R$  is in pm,  $M_X$  is the mass of a single ligand X in amu (e.g., 35.5 for Cl),  $\nu_s$  is the symmetric breathing vibrational frequency of the final species in  $\text{cm}^{-1}$ , and  $w$  is the often mistakenly overlooked topological factor (for  $\text{AX}_6$  complexes of  $\text{O}_h$  symmetry,  $w = 6$ ). For one-electron detachment from  $\text{UCl}_6^{2-}$ , we obtained  $\Delta R(\text{U–Cl}) \approx 20$  pm without the  $w$  factor, and with  $w$  we have  $\Delta R \approx 8$  pm. This experimentally derived value using Eq. (1) agrees much better with the theoretical  $\Delta R$  value in Table VII. This result suggests that one can evaluate the PES band widths ( $\Delta E$ ) using the optimized U–Cl bond-length change ( $\Delta R$ ).

### B. The electronic structures of $\text{UCl}_6^{q-}$ ( $q = 1, 2$ )

The extra electron in  $\text{UCl}_6^-$  occupies the non-degenerate  $1a_{2u}$  MO (Fig. 3), which is not split by SO coupling and does not induce first-order JT distortion of the octahedral complex. We have verified computationally that no pseudo-JT distortion occurs either. The U-5f orbitals are split by the  $\text{O}_h$  ligand field and the SO-coupling in the  $\text{UCl}_6^-$  anion into five levels (Table VIII), spanning a range of nearly 1.5 eV. Optically dipole-forbidden, vibrationally induced transitions from  $5f(a_{2u}) \rightarrow 5f(t_{1u,2u})$  would appear in the near and mid-IR regions. The lowest excitation  $XE_{5/2u} \rightarrow aU_{3/2u}$  has indeed been observed near 0.5 eV in the IR spectra of various  $\text{U(V)X}_6^-$  species in condensed phases,<sup>8,11,71</sup> in reasonable comparison with 0.39 eV calculated in the current study (Table VIII). For the next three 5f-5f excitation energies of  $\text{UCl}_6^-$ , our theoretical data agree with the experimental data in the condensed phase within  $\sim 0.15$  eV, i.e., slightly better than the reported SO-CASSCF and SO-CASPT2 results in the literature<sup>9,70</sup> (deviations within 0.26 eV). The observed gap of 0.6 eV between bands X and A in the PES of  $\text{UCl}_6^{2-}$  corresponds approximately to the mean energy of transitions in  $\text{UCl}_6^-$  from the  $XE_{5/2u}$  ground state to the SO split levels  $aU_{3/2u}$  and  $aE_{5/2u}$  at the ground-state geometry of  $\text{UCl}_6^{2-}$ .

In the case of octahedral  $\text{UCl}_6^{2-}$  with two 5f electrons, the lowest energy with minimal electron repulsion is obtained for two f electrons in two different MOs of  $2t_{2u}$  symmetry (Fig. 3). The atomic  $f^2$  configuration gives rise to 91 determinantal wavefunctions, and all symmetry adapted states are heavily determinant-mixed. Further mixing is induced by the strong 2e-Coulomb, SO, and ligand-field interactions (Tables II and III). The SO-coupled ground state is of  $A_{1g}$  type and has AO populations corresponding to  $\text{U-5f}^2$  ( $t_{2u}^{1.34}a_{2u}^{0.43}t_{1u}^{0.23}$ ). This  $A_{1g}$  ground state is not subject to pseudo-JT distortion; our investigation on  $D_{3d}$  or  $D_{4h}$  distortions at the SR-DFT/PBE level revealed little U–Cl bond length and angle changes. The lowest energy detachments

TABLE IX. Bond distances (in pm), charges, orbital populations,  $\sigma$ - and  $\pi$ -orbitals, bond orders, and U–Cl covalency in  $\text{UCl}_6^{q-}$  ( $q = 0^+-2$ ).<sup>a</sup>

Species	$R_{\text{U-Cl}}$	$Q_{\text{U}}^{\text{Vor}},$ $Q_{\text{Cl}}^{\text{Vor}}$	$Q_{\text{U}}^{\text{NBO}},$ $Q_{\text{Cl}}^{\text{NBO}}$	U-5f, U-6d, U-7s	NLMO $_{\sigma}$ , NLMO $_{\pi}$	Bond order		
						NM, NBO	MBO, GJ	Cov, (NRT) (%)
$\text{UCl}_6$	247.1	2.71, −0.45	1.51, −0.25	3.49, 0.64, 0.31	83%Cl( $s^{16}p^{84}$ ) + 16%U( $s^{14}d^{16}f^{70}$ ), 89%Cl( $p\pi$ ) + 10%U( $d^{13}f^{87}$ )	1.54, 1.17	1.33, 1.45	41
$\text{UCl}_6^-$	254.6	2.62, −0.60	1.76, −0.46	3.18, 0.54, 0.29	88%Cl( $s^{22}p^{78}$ ) + 12%U( $s^{19}d^{19}f^{62}$ ), 93%Cl( $p\pi$ ) + 6%U( $d^{15}f^{85}$ )	1.49, 1.12	1.08, 1.22	34
$\text{UCl}_6^{2-}$	266.9	2.39, −0.73	2.11, −0.68	2.92, 0.42, 0.26	92%Cl( $s^{25}p^{75}$ ) + 8%U( $s^{26}d^{21}f^{53}$ ), 96%Cl( $p\pi$ ) + 3%U( $d^{20}f^{80}$ )	1.48, 1.07	0.80, 0.94	26

<sup>a</sup>Bond lengths ( $R_{\text{U-Cl}}$  in pm); Voronoi and Weinhold NBO atomic charges of U and Cl ( $Q_{\text{U,Cl}}^{\text{Vor,NBO}}$  in +e units); NBO atomic orbital populations U-5f,6d,7s; AO contributions to the U–Cl  $\sigma$  and  $\pi$  interactions (NLMO $_{\sigma}$  and NLMO $_{\pi}$ ); bond orders: upper entries of Nalewajski and Mrozek (NM) and of Mayer (MBO), lower entries of NBO and of Gopinathan and Jug (GJ); Weinhold NRT bond covalences (Cov). The NM bond indices were calculated from two-electron valence indices based on the partitioning of  $\text{tr}(\Delta P^2)$  and are referred to as a 4-index set.

of the  $X A_{1g}$  ground state of  $\text{U}(f^2)\text{Cl}_6^{2-}$  yield the lowest final states of  $\text{U}(f^1)\text{Cl}_6^-$ :  $X E_{5/2u}(f-1a_{2u-5/2})$ ,  $a U_{3/2u}(f-2t_{2u-3/2})$ ,  $a E_{5/2u}(f-2t_{2u-5/2})$ ,  $b U_{3/2u}(f-3t_{1u-3/2})$ , and  $a E_{1/2u}(f-3t_{1u-1/2})$  (Fig. 5 and Table V). Since the final  $(3t_{1u})^1$  states ( $b U_{3/2u}$  and  $a E_{1/2u}$ , indicated by dotted lines in Fig. 5) are of shake-up type and have low intensities in the PES, the gap of 0.6 eV between the observed PES bands X and A in Fig. 2 corresponds to the energy gap between spinor  $1a_{2u-5/2}$  and the average of  $2t_{2u-3/2,5/2}$  of  $\text{UCl}_6^-$ , representing the average of the first and second excitation energies of  $\text{UCl}_6^-$ , which are calculated at the ground-state geometry of  $\text{UCl}_6^{2-}$  as 0.34 eV and 0.73 eV (Table V), and observed as 0.5 and 0.85 eV in the IR region (Table VIII).

### C. Chemical bonding in $\text{UCl}_6^{q-}$ ( $q = 0-2$ )

The results of chemical bonding analyses are presented in Table IX. We have investigated two questions. First, how do the added electrons distribute over the molecules in the series  $\text{UCl}_6 \rightarrow \text{UCl}_6^- \rightarrow \text{UCl}_6^{2-}$ ? The expectation is that they go into the inner U-5f shell. We applied two different procedures to assign formal or effective electronic charges to the atoms. In the Voronoi procedure,<sup>91</sup> the bond is cut in the geometric middle of the bond line. Most of the added electronic charge goes to the outer region of the U atom, where the Cl atoms are overlapping (Table IX). As a result, by decreasing the oxidation state of U by 1 formal unit from  $\text{U}^{+6}$  to  $\text{U}^{+5}$  to  $\text{U}^{+4}$ , the positive Voronoi charge on the U atom decreases only by a small amount, i.e., by 0.09|e| and 0.23|e|, respectively, while the added electronic charge is dominantly assigned to the Cl anions, which become more negative by nearly  $-1/6$ . In the NBO procedure,<sup>92</sup> the electronic charge is assigned to the overlapping AOs. Here, the charge on the Cl atoms even varies slightly more than by  $-e/6$  upon reduction of the U cation by 1 formal unit. In other words, oxidizing the uranium halides implies removing electronic charge from the ligands rather than from the formally oxidized central metal.

This result suggests the second interesting aspect: how do ionicity and covalency change from  $\text{UCl}_6 \rightarrow \text{UCl}_6^- \rightarrow \text{UCl}_6^{2-}$  upon sequential reduction? The covalent bond

orders of Mayer<sup>93</sup> and of Gopinathan-Jug<sup>94</sup> decrease in this order. In contrast, the overall (covalent and ionic) bond order of Nalewajski-Mrozek<sup>95</sup> and the NBO of Weinhold *et al.*,<sup>92</sup> do not vary much, indicating a remarkable increase of ionic bonding in the counterintuitive order. Namely, from  $\text{U}(+6) \rightarrow \text{U}(+5) \rightarrow \text{U}(+4)$ , the effective positive charge on U varies very little, but the effective negative charge on the chlorine ligands increases substantially, so that the effective ionic product  $Q_{\text{U}}-Q_{\text{Cl}}$  increases from  $(\text{U}^{+6})(\text{Cl}^-)_6$  to  $(\text{U}^{+4})(\text{Cl}^-)_6$  counter-intuitively, independent of the charge definition (Voronoi or NBO). Also the NLMOs become more polar towards Cl, when electrons are formally added into the U-5f shell, thereby reducing the electron affinity of the central atom. The U-5f AOs have much larger percentage contribution in both  $\sigma$  and  $\pi$  dative bonding than the U-6d AOs, while the latter are more important in orbital overlap.

As shown in Fig. 3, the energies of the Cl-3p and U-5f valence shells approach each other upon oxidation from  $\text{U}^{+4}$  to  $\text{U}^{+6}$ . Namely, increasing the oxidation state of U lowers the energies of the metal orbitals and provides better chances for U–Cl interactions.<sup>8,17</sup> Oxidation of  $\text{UCl}_6^{2-}$  reduces the negative charge on the ligands and also the Coulomb repulsion between the ligands, thereby leading to shorter bond lengths (Table IX) and better orbital overlap. As a result, the U–Cl covalency increases from 26% in  $\text{UCl}_6^{2-}$  to 41% in  $\text{UCl}_6$ , i.e., uranium with higher oxidation state possesses larger covalent bonding.

## VII. CONCLUSIONS

We report the first experimental observation of  $\text{UCl}_6^-$  and  $\text{UCl}_6^{2-}$  in the gas phase and the investigation of their electronic structures by low-temperature photoelectron spectroscopy and by *ab initio* calculations. Both the first and second electron affinities of  $\text{UCl}_6$  are measured for the first time, as 5.3 eV and 0.60 eV, respectively. The open 5f shell together with the high electronegativity of the ligands contributes to the large electron affinity of  $\text{UCl}_6$ . The detachment cross section of the single 5f electron ( $5f_{xyz}^1$ ) in  $\text{UCl}_6^-$  was observed to be extremely small.

$UCl_6^{2-}$  with two 5f electrons is found to possess a strong multi-determinantal ground state, giving rise to multiple detachment features beyond Koopmans' theorem. Multi-reference WFT *ab initio* methods with spin-orbit coupling are necessary to accurately interpret the detailed electronic structures of these uranium hexachloride species. The U–Cl covalency is found to decrease upon reduction of formal ionicity from  $[(U^{+6})Cl_6] \rightarrow [(U^{+5})Cl_6]^- \rightarrow [(U^{+4})Cl_6]^{2-}$ .

## ACKNOWLEDGMENTS

This material is based on the work supported by the U.S. Department of Energy, Office of Science, Office of Basic Energy Sciences under Award No. DE-SC0006979 (to L.S.W.). The theoretical work was supported by NSF of China (21433005, 21201106) and the “Strategic Priority Research Program” of the Chinese Academy of Sciences (Grant No. XDA02040104) and the National Basic Research Program of China (Grant No. 2010CB934504) and the Program of International S&T Cooperation (2014DFG60230, ANSTO-SINAP). The calculations were performed at the Supercomputer Center of the Computer Network Information Center, Chinese Academy of Sciences, and Tsinghua National Laboratory for Information Science and Technology. A portion of the calculations was performed using EMSL, a national scientific user facility sponsored by the U.S. Department of Energy's Office of Biological and Environmental Research and located at the Pacific Northwest National Laboratory, USA.

<sup>1</sup>N. Kaltsoyannis and B. E. Bursten, *Inorg. Chem.* **34**, 2735 (1995).

<sup>2</sup>M. Pepper and B. E. Bursten, *Chem. Rev.* **91**, 719 (1991).

<sup>3</sup>R. Arratia-Pérez, L. Hernandez-Acevedo, and G. L. Malli, *J. Chem. Phys.* **121**, 7743 (2004); H. Xiao and J. Li, *Chin. J. Struct. Chem.* **27**, 967 (2008), available at [http://d.wanfangdata.com.cn/Periodical\\_jghx200808010.aspx](http://d.wanfangdata.com.cn/Periodical_jghx200808010.aspx).

<sup>4</sup>T. Nagai, A. Uehara, T. Fujii, N. Sato, and H. Yamana, *IOP Conf. Ser.: Mater. Sci. Eng.* **9**, 012050 (2010).

<sup>5</sup>T. Nagai, A. Uehara, T. Fujii, O. Shirai, N. Sato, and H. Yamana, *Electrochem.* **77**, 614 (2009).

<sup>6</sup>I. B. Polovov, V. A. Volkovich, J. M. Charnock, B. Kralj, R. G. Lewin, H. Kinoshita, I. May, and C. A. Sharrad, *Inorg. Chem.* **47**, 7474 (2008).

<sup>7</sup>S. I. Nikitenko, C. Cannes, C. Le Naour, P. Moisy, and D. Trubert, *Inorg. Chem.* **44**, 9497 (2005).

<sup>8</sup>W. W. Lukens, N. M. Edelstein, N. Magnani, T. W. Hayton, S. Fortier, and L. A. Seaman, *J. Am. Chem. Soc.* **135**, 10742 (2013).

<sup>9</sup>F. P. Notter and H. Bolvin, *J. Chem. Phys.* **130**, 184310 (2009).

<sup>10</sup>L. A. Seaman, G. Wu, N. Edelstein, W. W. Lukens, N. Magnani, and T. W. Hayton, *J. Am. Chem. Soc.* **134**, 4931 (2012).

<sup>11</sup>J. Selbin, J. D. Ortego, and G. Gritzner, *Inorg. Chem.* **7**, 976 (1968).

<sup>12</sup>L. Ryan, *J. Inorg. Nucl. Chem.* **33**, 153 (1971).

<sup>13</sup>N. Edelstein, D. Brown, and B. Whitaker, *Inorg. Chem.* **13**, 563 (1974).

<sup>14</sup>J. Selbin and H. J. Sherrill, *Inorg. Chem.* **13**, 1235 (1974).

<sup>15</sup>G. Thornton, N. Edelstein, and N. Rösch, *J. Chem. Phys.* **70**, 5218 (1979).

<sup>16</sup>G. Thornton, N. Rösch, and N. Edelstein, *Inorg. Chem.* **19**, 1304 (1980).

<sup>17</sup>S. G. Minasian, J. M. Keith, E. R. Batista, K. S. Boland, D. L. Clark, S. D. Conradson, S. A. Kozimor, R. L. Martin, D. E. Schwarz, D. K. Shuh, G. L. Wagner, M. P. Wilkerson, L. E. Wolfsberg, and P. Yang, *J. Am. Chem. Soc.* **134**, 5586 (2012).

<sup>18</sup>L. R. Morss, N. M. Edelstein, and J. Fuger, *The Chemistry of the Actinide and Transactinide Elements* (Springer, Dordrecht, 2006), Vol. 1.

<sup>19</sup>S. G. Minasian, K. S. Boland, R. K. Feller, A. J. Gaunt, S. A. Kozimor, I. May, S. D. Reilly, B. L. Scott, and D. K. Shuh, *Inorg. Chem.* **51**, 5728 (2012).

<sup>20</sup>S. Siegel, *Acta Cryst.* **9**, 827 (1956).

<sup>21</sup>E. Staritzky and J. Singer, *Acta Cryst.* **5**, 536 (1952).

<sup>22</sup>L. S. Wang, C. F. Ding, X. B. Wang, and S. E. Barlow, *Rev. Sci. Instrum.* **70**, 1957 (1999).

<sup>23</sup>X. B. Wang and L. S. Wang, *Rev. Sci. Instrum.* **79**, 073108 (2008).

<sup>24</sup>H. T. Liu, C. G. Ning, D. L. Huang, P. D. Dau, and L. S. Wang, *Angew. Chem., Int. Ed.* **52**, 8976 (2013); H. T. Liu, C. G. Ning, D. L. Huang, and L. S. Wang, *Angew. Chem., Int. Ed.* **53**, 2464 (2014); D. L. Huang, P. D. Dau, H. T. Liu, and L. S. Wang, *J. Chem. Phys.* **140**, 224315 (2014).

<sup>25</sup>P. D. Dau, J. Su, H. T. Liu, J. B. Liu, D. L. Huang, J. Li, and L. S. Wang, *Chem. Sci.* **3**, 1137 (2012).

<sup>26</sup>P. D. Dau, J. Su, H. T. Liu, D. L. Huang, J. Li, and L. S. Wang, *J. Chem. Phys.* **137**, 064315 (2012).

<sup>27</sup>J. Su, P. D. Dau, Y. H. Qiu, H. T. Liu, C. F. Xu, D. L. Huang, L. S. Wang, and J. Li, *Inorg. Chem.* **52**, 6617 (2013).

<sup>28</sup>P. D. Dau, J. Su, H. T. Liu, D. L. Huang, F. Wei, J. Li, and L. S. Wang, *J. Chem. Phys.* **136**, 194304 (2012).

<sup>29</sup>P. D. Dau, H. T. Liu, D. L. Huang, and L. S. Wang, *J. Chem. Phys.* **137**, 116101 (2012).

<sup>30</sup>W. L. Li, H. S. Hu, T. Jian, G. V. Lopez, J. Su, J. Li, and L. S. Wang, *J. Chem. Phys.* **139**, 244303 (2013).

<sup>31</sup>J. Su, P. D. Dau, C. F. Xu, D. L. Huang, H. T. Liu, F. Wei, L. S. Wang, and J. Li, *Chem. Asian J.* **8**, 2489 (2013).

<sup>32</sup>Y. H. Cho, S. E. Bae, Y. J. Park, S. Y. Oh, J. Y. Kim, and K. Song, *Microchem. J.* **102**, 18 (2012).

<sup>33</sup>H. T. Liu, Y. L. Wang, X. G. Xiong, P. D. Dau, Z. Piazza, D. L. Huang, C. Q. Xu, J. Li, and L. S. Wang, *Chem. Sci.* **3**, 3286 (2012).

<sup>34</sup>J. C. Rienstra-Kiracofe, G. S. Tschumper, H. F. Schaefer III, S. Nandi, and G. B. Ellison, *Chem. Rev.* **102**, 231 (2002).

<sup>35</sup>J. C. Ehrhardt and S. P. Davis, *J. Opt. Soc. Am.* **61**, 1342 (1971).

<sup>36</sup>C. G. Ning, X. G. Xiong, Y. L. Wang, J. Li, and L. S. Wang, *Phys. Chem. Chem. Phys.* **14**, 9323 (2012).

<sup>37</sup>J. P. Perdew, K. Burke, and M. Ernzerhof, *Phys. Rev. Lett.* **77**, 3865 (1996).

<sup>38</sup>ADF 2010.01, see <http://www.scm.com>.

<sup>39</sup>C. Fonseca Guerra, J. G. Snijders, G. te Velde, and E. J. Baerends, *Theor. Chem. Acc.* **99**, 391 (1998).

<sup>40</sup>G. te Velde, F. M. Bickelhaupt, E. J. Baerends, C. Fonseca Guerra, S. J. A. van Gisbergen, J. G. Snijders, and T. Ziegler, *J. Comput. Chem.* **22**, 931 (2001).

<sup>41</sup>E. van Lenthe and E. J. Baerends, *J. Comput. Chem.* **24**, 1142 (2003).

<sup>42</sup>E. van Lenthe, E. J. Baerends, and J. G. Snijders, *J. Chem. Phys.* **99**, 4597 (1993).

<sup>43</sup>A. D. Becke, *Phys. Rev. A* **38**, 3098 (1988).

<sup>44</sup>C. Lee, W. Yang, and R. G. Parr, *Phys. Rev. B* **37**, 785 (1988).

<sup>45</sup>P. R. T. Schipper, O. V. Gritsenko, S. J. A. van Gisbergen, and E. J. Baerends, *J. Chem. Phys.* **112**, 1344 (2000).

<sup>46</sup>H.-J. Werner, P. J. Knowles, G. Knizia, F. R. Manby, and M. Schütz, *WIREs Comput. Mol. Sci.* **2**, 242–253 (2012); H.-J. Werner, P. J. Knowles, G. Knizia, F. R. Manby, M. Schütz *et al.*, MOLPRO, version 2012.1, a package of *ab initio* programs, 2012, see <http://www.molpro.net>.

<sup>47</sup>M. Valiev, E. J. Bylaska, N. Govind, K. Kowalski, T. P. Straatsma, H. J. J. Van Dam, D. Wang, J. Nieplocha, E. Apra, T. L. Windus, and W. de Jong, *Comput. Phys. Commun.* **181**, 1477 (2010).

<sup>48</sup>C. Hampel, K. A. Peterson, and H.-J. Werner, *Chem. Phys. Lett.* **190**, 1 (1992); M. J. O. Deegan and P. J. Knowles, *Chem. Phys. Lett.* **227**, 321 (1994); P. J. Knowles, C. Hampel, and H.-J. Werner, *J. Chem. Phys.* **99**, 5219 (1993).

<sup>49</sup>H.-J. Werner, *Mol. Phys.* **89**, 645 (1996); P. Celani and H.-J. Werner, *J. Chem. Phys.* **112**, 5546 (2000).

<sup>50</sup>K. Kowalski and P. Piecuch, *J. Chem. Phys.* **120**, 1715 (2004).

<sup>51</sup>M. Dolg, see <http://www.tc.uni-koeln.de/PP/clickpse.en.html>.

<sup>52</sup>X. Cao, M. Dolg, and H. Stoll, *J. Chem. Phys.* **118**, 487 (2003).

<sup>53</sup>X. Cao and M. Dolg, *J. Mol. Struct. (Theochem)* **673**, 203 (2004).

<sup>54</sup>D. E. Woon and T. H. Dunning, *J. Chem. Phys.* **98**, 1358 (1993).

<sup>55</sup>P. Å. Malmqvist, B. O. Roos, and B. Schimmelpfennig, *Chem. Phys. Lett.* **357**, 230 (2002); B. O. Roos and P. Å. Malmqvist, *Phys. Chem. Chem. Phys.* **6**, 2919 (2004).

<sup>56</sup>X. B. Wang, Y. L. Wang, J. Yang, X. P. Xing, J. Li, and L. S. Wang, *J. Am. Chem. Soc.* **131**, 16368 (2009).

<sup>57</sup>Y. L. Wang, H. J. Zhai, L. Xu, J. Li, and L. S. Wang, *J. Phys. Chem. A* **114**, 1247 (2010).

<sup>58</sup>Y. L. Wang, X. B. Wang, Y. X. P. Xing, F. Wei, J. Li, and L. S. Wang, *J. Phys. Chem. A* **114**, 11244 (2010).

<sup>59</sup>H. T. Liu, X. G. Xiong, P. D. Dau, Y. L. Wang, J. Li, and L. S. Wang, *Chem. Sci.* **2**, 2101 (2011).

<sup>60</sup>J. Su, Y. L. Wang, F. Wei, W. H. E. Schwarz, and J. Li, *J. Chem. Theory Comput.* **7**, 3293 (2011).

<sup>61</sup>G. Ghigo, B. O. Roos, and P. A. Malmqvist, *Chem. Phys. Lett.* **396**, 142 (2004).

- <sup>62</sup>F. Weinhold and C. R. Landis, *Valency and Bonding. A Natural Bond Orbital Donor-Acceptor Perspective* (Cambridge University Press, Cambridge UK, 2005).
- <sup>63</sup>E. D. Glendening, J. K. Badenhoop, A. E. Reed, J. E. Carpenter, J. A. Bohmann, C. M. Morales, C. R. Landis, and F. Weinhold, NBO 6.0 (Theoretical Chemistry Institute of the University of Wisconsin, Madison WI, 2013).
- <sup>64</sup>M. J. Frisch *et al.*, GAUSSIAN 09, Revision B.01 (Gaussian, Inc., Wallingford CT 2010).
- <sup>65</sup>X. B. Wang, C. F. Ding, and L. S. Wang, *Chem. Phys. Lett.* **307**, 391 (1999); X. B. Wang and L. S. Wang, *Phys. Rev. Lett.* **83**, 3402 (1999).
- <sup>66</sup>U. Berzins, M. Gustafsson, D. Hanstorp, A. Klinkmüller, U. Ljungblad, and A. M. Mårtensson-Pendrill, *Phys. Rev. A* **51**, 231 (1995).
- <sup>67</sup>The spectroscopic SO splitting of Cl-3p (i.e., 0.1094 eV) is from the National Institute of Standards and Technology (NIST) data base.
- <sup>68</sup>X. B. Wang, C. F. Ding, and L. S. Wang, *Phys. Rev. Lett.* **81**, 3351 (1998); L. S. Wang, C. F. Ding, X. B. Wang, J. B. Nicholas, and B. Nicholas, *Phys. Rev. Lett.* **81**, 2667 (1998); X. B. Wang and L. S. Wang, *Nature* **400**, 245 (1999); X. B. Wang and L. S. Wang, *Ann. Rev. Phys. Chem.* **60**, 105 (2009).
- <sup>69</sup>See supplementary material at <http://dx.doi.org/10.1063/1.4916399> for the listing of the calculated VDEs for  $\text{UCl}_6^-$  and  $\text{UCl}_6^{2-}$  and two different notations for the irreducible representations of double group  $\text{O}_h^9$ .
- <sup>70</sup>D. Ganyushin and F. Neese, *J. Chem. Phys.* **138**, 104113 (2013).
- <sup>71</sup>K. Eichberger and F. Lux, *Ber. Bunsenges. Phys. Chem.* **84**, 800 (1980).
- <sup>72</sup>D. Johnston, R. Satten, and E. Wong, *J. Chem. Phys.* **44**, 687 (1966).
- <sup>73</sup>R. A. Satten, C. L. Schreiber, and E. Y. Wong, *J. Chem. Phys.* **42**, 162 (1965).
- <sup>74</sup>C. D. Flint and P. A. Tanner, *Mol. Phys.* **61**, 389 (1987).
- <sup>75</sup>D. R. Johnston, R. A. Satten, C. L. Schreiber, and E. Y. Wong, *J. Chem. Phys.* **44**, 3141 (1966).
- <sup>76</sup>R. A. Satten, C. L. Schreiber, and E. Y. Wong, *J. Chem. Phys.* **78**, 79 (1983).
- <sup>77</sup>D. E. Bugaris and J. A. Ibers, *J. Solid State Chem.* **181**, 3189 (2008).
- <sup>78</sup>E. Bossé, C. Den Auwer, C. Berthon, P. Guilbaud, M. S. Grigoriev, S. Nikitenko, C. Le Naour, C. Cannes, and P. Moisy, *Inorg. Chem.* **47**, 5746 (2008).
- <sup>79</sup>J. C. Taylor and P. W. Wilson, *Acta Crystallogr., Sect. B: Struct. Crystallogr. Cryst. Chem.* **30**, 1481 (1974).
- <sup>80</sup>S. I. Nikitenko, C. Hennig, M. S. Grigoriev, C. Le, C. Naour, D. Cannes, E. Trubert, C. Bossé, P. Berthon, and Moisy, *Polyhedron* **26**, 3136 (2007).
- <sup>81</sup>W. Kolitsch and U. Müller, *Z. anorg. allg. Chem.* **410**, 21 (1974).
- <sup>82</sup>P. J. Bendall, *J. Appl. Cryst.* **16**, 164 (1983).
- <sup>83</sup>J. C. Taylor and A. B. Waugh, *Polyhedron* **2**, 211 (1983).
- <sup>84</sup>J. Shamir and A. Silberstein, *J. Inorg. Nucl. Chem.* **37**, 1173 (1975).
- <sup>85</sup>W. Kolitsch and U. Müller, *Z. anorg. allg. Chem.* **418**, 235 (1975).
- <sup>86</sup>R. M. Badger, *J. Chem. Phys.* **2**, 128 (1934); R. M. Badger, *Phys. Rev.* **48**, 284 (1935); R. M. Badger, *J. Chem. Phys.* **3**, 710 (1935).
- <sup>87</sup>W. L. Li, J. Su, T. Jian, G. V. Lopez, H. S. Hu, G. J. Cao, J. Li, and L. S. Wang, *J. Chem. Phys.* **140**, 094306 (2014).
- <sup>88</sup>M. S. Miao, *Nat. Chem.* **5**, 846 (2013).
- <sup>89</sup>S. Riedel and P. Schwerdtfeger, *Nat. Chem.* **5**, 815 (2013).
- <sup>90</sup>J. Su, F. Wei, W. H. E. Schwarz, and J. Li, *J. Phys. Chem. A* **116**, 12299 (2012).
- <sup>91</sup>C. F. Guerra, J.-W. Handgraaf, E. J. Baerends, and F. M. Bickelhaupt, *J. Comput. Chem.* **25**, 189 (2004).
- <sup>92</sup>A. E. Reed, L. A. Curtiss, and F. Weinhold, *Chem. Rev.* **88**, 899 (1988).
- <sup>93</sup>I. Mayer, *Chem. Phys. Lett.* **97**, 270 (1983).
- <sup>94</sup>M. S. Gopinathan and K. Jug, *Theor. Chim. Acta* **63**, 497 (1983).
- <sup>95</sup>A. Michalak, R. L. DeKock, and T. Ziegler, *J. Phys. Chem. A* **112**, 7256 (2008); R. F. Nalewajski and J. Mrozek, *Int. J. Quantum Chem.* **51**, 187 (1994); R. F. Nalewajski and J. Mrozek, *Int. J. Quantum Chem.* **61**, 589 (1997); R. F. Nalewajski, J. Mrozek, and A. Michalak, *Polish J. Chem.* **72**, 1779 (1998); R. F. Nalewajski, J. Mrozek, and G. Mazur, *Can. J. Chem.* **74**, 1121 (1996).
- <sup>96</sup>E. J. Baerends, O. V. Gritsenko, and R. van Meer, *Phys. Chem. Chem. Phys.* **15**, 16408 (2013); R. van Meer, O. V. Gritsenko, and E. J. Baerends, *J. Chem. Theory Comput.* **10**, 4432 (2014).